ornl

ORNL/TM-12474

OAK RIDGE
NATIONAL
LABORATORY

MARTIN MARIETTA

Development of a Three-Dimensional Groundwater Flow Model for Western Melton Valley: Application of P-FEM on a DOE Waste Site

OAK RIDGE NATIONAL LABORATORY
CENTRAL RESEARCH LIBRARY
CIRCULATION SECTION
4500N ROOM 175
LIBRARY LOAN COPY
DO NOT TRANSFER TO ANOTHER PERSON
If you wish someone else to see this report, send in name with report and the library will arrange a loan.

O. R. West
L. E. Toran

Environmental Sciences Division
Publication No. 4268

MANAGED BY
MARTIN MARIETTA ENERGY SYSTEMS, INC.
FOR THE UNITED STATES
DEPARTMENT OF ENERGY

This report has been reproduced directly from the best available copy.

Available to DOE and DOE contractors from the Office of Scientific and Technical Information, P.O. Box 62, Oak Ridge, TN 37831; prices available from (615) 576-8401, FTS 626-8401.

Available to the public from the National Technical Information Service, U.S. Department of Commerce, 5285 Port Royal Rd., Springfield, VA 22161.

This report was prepared as an account of work sponsored by an agency of the United States Government. Neither the United States Government nor any agency thereof, nor any of their employees, makes any warranty, express or implied, or assumes any legal liability or responsibility for the accuracy, completeness, or usefulness of any information, apparatus, product, or process disclosed, or represents that its use would not infringe privately owned rights. Reference herein to any specific commercial product, process, or service by trade name, trademark, manufacturer, or otherwise, does not necessarily constitute or imply its endorsement, recommendation, or favoring by the United States Government or any agency thereof. The views and opinions of authors expressed herein do not necessarily state or reflect those of the United States Government or any agency thereof.

ORNL/TM-12474

Environmental Sciences Division

DEVELOPMENT OF A THREE-DIMENSIONAL GROUNDWATER FLOW MODEL FOR WESTERN MELTON VALLEY: APPLICATION OF P-FEM ON A DOE WASTE SITE

O. R. West and L. E. Toran

Environmental Sciences Division
Publication No. 4268

Date Published: April 1994

Prepared for
U.S. Department of Energy
Office of Scientific Computing
under budget and reporting code KC 07 01 03 0

Prepared by
OAK RIDGE NATIONAL LABORATORY
Oak Ridge, Tennessee 37831-6285
Managed by
MARTIN MARIETTA ENERGY SYSTEMS, INC.
for the
U.S. DEPARTMENT OF ENERGY
under contract DE-AC05-84OR21400

MARTIN MARIETTA ENERGY SYSTEMS LIBRARIES

3 4456 0421628 4

CONTENTS

	Page
TABLES	v
FIGURES	vii
ACKNOWLEDGMENTS	ix
1. INTRODUCTION	1
1.1 BACKGROUND	1
1.2 OBJECTIVES AND SCOPE	1
2. BACKGROUND INFORMATION FOR GROUNDWATER MODEL DEVELOPMENT	3
2.1 MODEL REGION	3
2.2 CALIBRATION DATA SETS	3
2.3 HYDRAULIC CONDUCTIVITIES	9
2.4 PRECIPITATION AND RECHARGE	12
3. DEVELOPMENT AND CALIBRATION OF GROUNDWATER FLOW MODEL	13
3.1 MODEL CONSTRUCTION	13
3.2 BOUNDARY CONDITIONS	18
3.3 MATERIAL PROPERTIES: LAYERING	18
3.4 CALIBRATION PROCEDURES	20
4. RESULTS	21
4.1 SHALLOW PIEZOMETER CALIBRATION AND COMPARISON TO DEEP PIEZOMETER DATA	21
4.2 SELECTED ALTERNATE MODELS	27
4.3 EFFECTS OF CAPS IN WAG 6	28
4.4 COMPARISON OF LARGE- AND SMALL-SCALE MODELS OF WAG 6	32
5. RECOMMENDATIONS FOR FUTURE WORK	35
6. CONCLUSIONS	36
7. REFERENCES	37

LIST OF TABLES

Table		Page
1	Location and data summary of piezometers used in calibration	3
2	Hydraulic conductivities measured in Waste Area Grouping 6	10
3	Comparison of root mean square error (RMSE) and flux to West Seep for several model runs	27
4	Comparison of modeled flux (in cubic feet per second) to ungaged portion of Waste Area Grouping 6 for alternate models	34

LIST OF FIGURES

Figure		Page
1	Location of waste area groupings (WAGs) in the Western Melton Valley model	2
2	Location of calibration piezometers (represented by dots) in the Western Melton Valley model area	8
3	Finite-element surface grid on the topographic surface of the model, showing boundary conditions	14
4	Full three-dimensional, finite-element grid produced by the preprocessing routine from the surface grid generated by I-Deas	15
5	Diagram of the preprocessing program used to generate model input	16
6	Diagram of the postprocessing program used to visualize model output	17
7	Cross section showing hydraulic conductivity layers in the model	19
8	Modeled water level vs measured water level in shallow calibration data set	23
9	Map of degree of model error in piezometers selected for calibration	24
10	North-South cross section through White Oak Lake showing flow vectors	25
11	Bar chart of measured and modeled stream fluxes for four gaged stations in WAG 6	26
12	Location of piezometers (dots) used to compare alternate models and stream gages (triangles) used in Fig. 11	29
13	Head values in selected piezometers for alternate models	30
14	Comparison of capped and bare-ground models: (a) location of caps, (b) vector plots for bare ground, and (c) vector plots for capped conditions	31
15	Map of sections used to calculate fluxes along the ungaged perimeter of WAG 6	34

ACKNOWLEDGMENTS

This work was supported by the Office of Scientific Computing, U.S. Department of Energy, under contract DE-AC05-84OR21400 with Martin Marietta Energy Systems, Inc., and by the Oak Ridge National Laboratory Environmental Restoration Program.

Ed D'Azevedo created a parallel version of 3DFEMWATER for this project and provided training on using the parallel processing machine. Without his support, the work could not have been done. We would like to thank Mary Alice Wood who, is a member of the Oak Ridge Environmental Information System support staff, for her valuable assistance. She provided us with data files and maps that were needed for constructing the groundwater model.

1. INTRODUCTION

1.1 BACKGROUND

Modeling the movement of hazardous waste in groundwater was identified by the U.S. Department of Energy (DOE) as one of the "grand challenges" in scientific computation. In recognition of this need, DOE has provided support for a group of scientists from several national laboratories and universities to conduct research and development in groundwater flow and contaminant transport modeling. This group is part of a larger consortium of researchers, collectively referred to as the Partnership in Computational Science (PICS), that has been charged with the task of applying high-performance computational tools and techniques to "grand challenge" areas identified by DOE.

One of the goals of the PICS Groundwater Group is to develop a new three-dimensional groundwater flow and transport code that is optimized for massively parallel computers. An existing groundwater flow code, 3DFEMWATER, was "parallelized" in order to serve as a benchmark for these new models. The application of P-FEM, the parallelized version of 3DFEMWATER, to a real field site is the subject of this report.

1.2 OBJECTIVES AND SCOPE

A 3-dimensional, 40,000-node groundwater flow model of Melton Valley was constructed to understand the role of groundwater in contaminant discharge. Although the model does not account for dispersion of contaminants, it is useful for identifying groundwater pathways, recharge and discharge points, and groundwater fluxes to streams. The last can be used to estimate off-site contaminant fluxes. This modeling effort addresses saturated, steady-state flow conditions. Other efforts exist to model unsaturated flow and stormflow. Without a good model of the saturated flow system, neither contaminant transport nor transient problems such as alterations due to remediation can be modeled.

The site selected for the application of P-FEM is Western Melton Valley, which includes Waste Area Grouping (WAG) 6 (Fig. 1), the only operational low-level waste disposal facility at Oak Ridge National Laboratory (ORNL). Because of concern over off-site migration of hazardous wastes, WAG 6 and other waste area groupings within the Oak Ridge Reservation (Fig. 1) have been the subject of extensive site characterization and environmental monitoring activities. Calibration of the Melton Valley groundwater flow model is based on the substantial amount of data that has been collected from regular monitoring of piezometer and water quality wells installed within and around the ORNL waste areas.

In addition, the Melton Valley groundwater model was used to investigate the effects of capping burial areas. Proponents of this approach to remediating WAG 6 claim that the caps will lower the water table and prevent hazardous wastes in burial trenches from

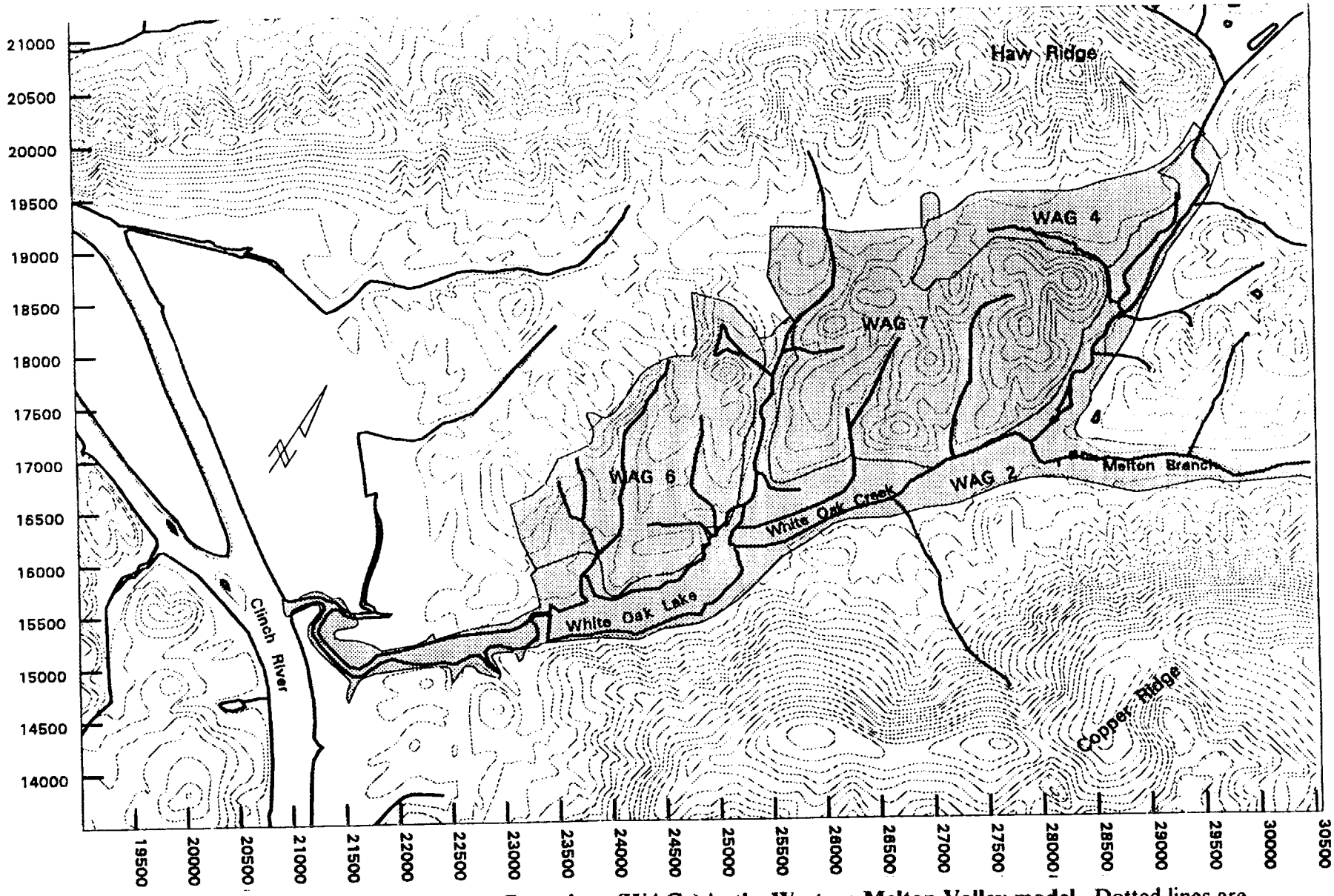

Figure 1. Location of Waste Area Groupings (WAGs) in the Western Melton Valley model. Dotted lines are topographic contours; outlines of the shaded areas are waste area boundaries; and heavy solid lines delineate lakes, rivers, and streams.

coming in contact with the groundwater. The groundwater flow model was used to test this hypothesis.

2. BACKGROUND INFORMATION FOR GROUNDWATER MODEL DEVELOPMENT

2.1 MODEL REGION

The Melton Valley groundwater model covers an area of about 50,477,000 ft^2 and is bounded on the north by Haw Ridge, on the south by Copper Ridge, on the east by the Clinch River, and on the west by the north trending branch of White Oak Creek. Since WAG 6 is located at the center of this model region, any uncertainties associated with specifying conditions at the model boundary are less likely to significantly affect flows calculated within WAG 6. The bottom of the model was set at an elevation of 200 ft above sea level (ASL) because very little data exists below this depth and measured hydraulic conductivities indicate that the flows at this depth are not active relative to the shallower groundwater flow system. Because the lowest topographic point within the region is at ~740 ft ASL, the minimum thickness of the model is about 540 ft. Steady-state conditions were assumed for the WAG 6 groundwater model, and fluctuations of water levels are typically less than 10 ft (Table 1).

The reference grid used throughout this report is the ORNL administrative grid system, which is rotated at 34° 12' 51" west with respect to true North. North refers to ORNL north, east to ORNL east, etc. The coordinate system coincides with the administrative grid system; i.e., the positive x-axis is directed towards the east and the positive y-axis directed towards the north. The z-coordinates correspond to elevations above sea level.

2.2 CALIBRATION DATA SETS

Two sets of piezometer data were used to calibrate the groundwater model. The first set was obtained from the Oak Ridge Environmental Information System (OREIS) data base and consists of water level measurements made on piezometers located within the model domain (Fig. 2). The piezometers selected for calibration (Table1) are a subset of the available piezometers which was selected for (a) availability of construction information, (b) distribution of locations across the domain (to avoid weighting results to clusters of piezometers), and (c) length of the data record. The second calibration data set was obtained from the hydraulic head measuring stations (HHMS) (Dreier and Toran 1989), which have been monitored monthly since 1988. A few piezometers were excluded from the calibration data set because they have not recovered (HHMS-4A, HHMS-5A, and HHMS-8A), were not monitored regularly (HHMS-8C), or are outside of the model region (HHMS-10 and HHMS-11). Even though the data from HHMS-6A are limited,

Table 1. Location and data summary of piezometers used in calibration

WELL #	NORTHING	EASTING	BOTTOM ELEV,FT	WATER LEV ELEV,FT	# OBS	S.D.
1050	21155	15752	730.62	745.44	18	2.28453
1054	21230	14761	728.9	740.312	19	1.30549
1053	21234	15045	729.75	739.411	18	1.44315
U19	21396.1	15888.2	731.7	743.748	948	0.7169
1056	21442	14913	732.71	740.932	19	2.32566
1055	21534	15693	736.32	741.197	18	0.78737
1057	21538	14726	732.87	742.347	19	1.5006
1058	21543	15304	704.05	740.784	18	0.87612
1059	21543	15321	730.87	741.817	25	1.40317
U18	21609.1	16354.1	731.1	745.214		
1060	21782	15466	730.78	741.055	18	0.89889
UB2	22059.2	17026.2	640.9	747.89		
UB1	22183.8	17064.4	731.2	750.847		
1065	22196	14733	705.53	745.496	19	1.75598
1061	22361	15534	712.95	747.841	18	1.70874
1064	22371	14929	720.67	740.406	19	1.14094
1062	22372	15552	743.99	747.979	18	1.3347
1068	22664	15436	731.3	745.355	17	0.49158
U16	22706.5	16957.7	746.9	769.015		
1067	22767	14945	724.39	742.529	18	0.6978
267	23221	16118	778.33	778.206	40	4.3569
743	23249	15098	739.7	744.559	37	1.96814
377	23297	16610	787.06	795.641	62	2.71386
268	23307	16365	790.76	792.453	68	5.5412
742	23339	15304	725.8	741.785	20	1.273
274	23347	16210	774.27	772.576	74	2.5437
741	23352	15597	741.31	745.071	38	0.93366
740	23372	15779	748.3	749.456	45	1.8795
744	23439	15165	736.37	745.191	37	1.57136
376	23479	16584	777.75	785.769	62	1.72411
375	23531	16935	793.37	794.1	61	1.32113
739	23604	15629	731.86	745.571	37	0.79165
273	23633	16126	757.24	758.139	66	0.7695
365	23681	16454	768.08	765.556	91	0.65561
364	23838	16407	766.02	764.221	80	3.07111
276	23895	16211	758.92	757.65	91	1.1717
311	23900	16936	786.41	782.961	51	1.8459
641	23985.2	17383.5	791.29	818.66	51	2.58658
295	23992	16703	773.6	773.206	76	1.6065
642	24035.6	16581	754.53	770.37	131	1.87466
653	24070	15793	708.54	746.748	126	0.90503
638	24119.4	17495.1	785.86	801.95	51	2.00075
637	24136	17715.1	801.92	805.77	51	2.49043
277	24182	16207	758.69	757.349	88	2.8557
643	24204.8	16344.4	759.42	760.78	10	1.00764
636	24326.2	17668	786.53	802.75	124	1.86555
TR-10	24348	15881		750.818	91	2.28979
384	24377	16131	751.55	754.885	57	2.24092
107	24402	17041	694.81	789.207	91	1.51104
356	24451	16481	769.06	761.68	88	1.99538
648	24524.2	17374.6	783.42	798.95	72	1.72058
346	24631	16435	761.42	763.332	86	2.1265

Table 1. (Continued)

WELL #	NORTHING	EASTING	BOTTOM ELEV,FT	WATER LEV ELEV,FT	# OBS	S.D.
1003	24668.2	16782.5	713.09	777.64	209	0.75504
656	24693	17923.9	737.59	809.23	117	2.96149
640	24719.6	17614.7	783.34	802.64	76	2.17877
647	24749	17145.7	785.67	787.64	71	0.63224
655	24815.3	17469.7	725.79	798.63	118	1.7894
644	24848.4	16748.9	764.3	770.31	272	1.06914
359	24867	16904	773.16	777.557	82	1.81796
652	24900	16159.7	690.16	748.44	43	0.84097
1166	24945.9	17697.2	780.01	794.03	165	0.88394
370	24981	17145	778.83	786.069	64	1.17269
1164	24993.1	17814.5	780.05	789.11	261	0.71762
372	25042	16570	746.84	759.495	58	1.67206
747	25065	15488	736.64	746.886	19	1.54341
649	25075.5	17375.5	791.97	794.45	77	0.78824
371	25090	16393	741.56	746.32	64	0.83172
1158	25102.5	17816.1	786.8	788.71	298	1.21444
1163	25141.2	17689.5	786.68	790.37	190	1.89833
651	25190.7	16870.9	703.82	766	43	0.74216
645	25274.6	17173.7	744.78	758.7	116	0.77022
1168	25295.2	17645.7	764.71	772.5	165	1.35928
374	25346	17462	756.39	763.449	63	2.10806
90	25473	16782		746.79	34	1.94149
738	25498.8	16134.2	739.77	744.29	10	0.39721
748	25535	15891	741.29	749.152	10	0.72507
95	25542	17209		755.58	24	0.67291
T401	25586	17454		761.15	24	1.52372
104	25660	16957		755.33	23	1.24632
126	25698	17779		765.96	34	3.46304
88	25746	16695		745.97	24	2.10595
103	25760	17074		767.162	23	1.56902
T411	25798	17299		769.13	24	0.6415
70	25834	18719		792.266	24	2.28352
735	25907.1	16707.9	741.54	745.466	14	1.69336
T403	25917	17703		788.236	24	1.98206
65	25945	18988		802.035	48	3.93681
94	25985	16960		756.315	24	1.42018
737	25992.6	16434.9	740.63	744.914	14	0.9367
125	25995	17874		782.74	24	1.04767
86	26009	16808		749.04	25	2.02191
749	26038.6	16314.9	741.86	745.619	15	0.1657
124	26079	17916		786.532	24	0.84408
T405	26098	17556		785.395	33	1.87301
67	26136	18468		777.055	33	1.85117
83	26191	17285		767.865	24	0.2693
84	26224	17162		762.69	48	0.42012
85	26252	16910		752.932	25	0.51605
64	26277	19215		809.827	33	2.723
WT5-8	26328	17065		758.339	33	0.51463
114	26433	18148		804.919	48	2.19873
WT5-3	26439	17358		771.925	24	0.94864
97	26453	17598		776.426	32	0.76293
98	26531	17715		778.725	23	1.53467
99	26575	17777		782.15	23	1.34368
731	26601.1	16821.5	744.59	748.728	19	1.84346

Table 1. (Continued)

WELL #	NORTHING	EASTING	BOTTOM ELEV,FT	WATER LEV ELEV,FT	# OBS	S.D.
U26	26803	17013.4	748.7	751.32	1007	1.0645
576	26805	18796.9	782.84	797.122	31	1.46366
183	26997	18612		837.742	75	1.95949
679	27001.9	19429.4	786.78	812.516	24	1.84285
690	27060.5	19009.8	802.22	815.958	37	3.70001
680	27320.2	18820.1	814.89	826.709	32	2.68266
186	27549	19019	792.79	791.682	76	0.17104
T7-29	27698.2	17638.4		777.413	31	1.99736
T7-25	27709.4	17483.1		767.342	31	0.75918
404	27714	19220	790.5	793.774	50	0.54619
678	27727.6	18663.2	778.71	821.226	25	2.0234
4TR-4	27777	19548		831.554	92	3.47924
WT7-3	27785	17223		761.653	46	1.59098
T6-1	27795	18731		833.823	33	6.73079
WT7-7	27822	17512		765.771	17	1.47584
720	27839.8	18821.2	789.32	814.941	10	1.21568
U27	27980.8	17441.7	754.5	753.285	1022	1.1527
T6-3	28005	18691		833.455	33	1.22743
685	28049.7	19399.8	769.59	806.12	52	1.40175
686	28050.4	19200.1	754.77	789.312	52	0.83385
684	28065.8	19602.2	792.48	825.53	34	4.85676
771	28516.2	18118.4	716.91	756.047	13	1.26148
203	28572	19001	777.29	778.46	54	1.6132
688	28798.6	19121.6	764.71	777.358	37	0.48983
682	28840	19469.8	768.2	790.612	37	2.12672
787	28890.6	18954.1	756.46	761.29	11	1.43168
689	29159.3	19339.9	756.87	774.767	37	1.23543
A-24	29198	19205	764.9	761.974	72	0.62873
A-35	29296	19598	770.52	766.926	75	0.42339
U30	29668.3	19962.3	764	770.083	1051	0.7195

Table 1. (Continued)

(Water levels are averages of monthly readings from 1990 through August 1992)

Well Label	Easing (feet)	Northing (feet)	Screened Interval (feet ASL)	Well Depth (feet)	Number of Observations	Average Water Level (feet ASL)	S.D.
HHMS-1A	27964.36	18014.84	470.11	400.00	29	786.58	0.48
HHMS-1B	27966.49	17989.34	668.88	201.20	29	796.79	3.24
HHMS-1C	27976.47	17963.94	768.84	101.00	29	801.83	4.55
HHMS-2A	27562.33	17225.06	406.00	400.50	29	759.48	0.89
HHMS-2B	27535.95	17214.92	607.18	200.50	29	756.24	0.44
HHMS-2C	27510.61	17208.13	726.26	81.10	29	753.23	0.55
HHMS-3A	26724.48	17213.80	419.69	399.10	29	773.28	0.72
HHMS-3B	26705.25	17195.99	607.31	211.50	29	766.30	0.47
HHMS-3C	26689.95	17175.96	737.48	80.50	29	769.24	1.12
HHMS-4B	24688.37	16148.20	572.48	215.30	29	754.52	0.49
HHMS-4C	24676.08	16170.59	726.36	61.50	29	754.54	0.97
HHMS-5B	24595.29	15827.63	546.93	219.50	28	750.58	0.48
HHMS-5C	24561.12	15833.46	703.79	63.00	28	745.80	0.48
HHMS-6B	24745.16	15289.25	596.87	165.40	29	745.95	0.49
HHMS-6C	24732.51	15268.72	701.67	60.80	29	750.91	1.27
HHMS-7A	24512.09	17540.65	406.04	402.50	29	789.24	0.10
HHMS-7B	24509.40	17518.90	513.64	295.00	29	791.66	0.43
HHMS-7C	24506.56	17498.37	630.76	178.00	29	799.59	1.03
HHMS-8B	24697.05	16810.70	586.53	197.00	29	779.25	1.36
HHMS-9B	27904.42	18809.57	621.25	238.00	29	788.86	0.60
HHMS-9C	27875.83	18815.87	780.87	80.00	29	818.19	1.02

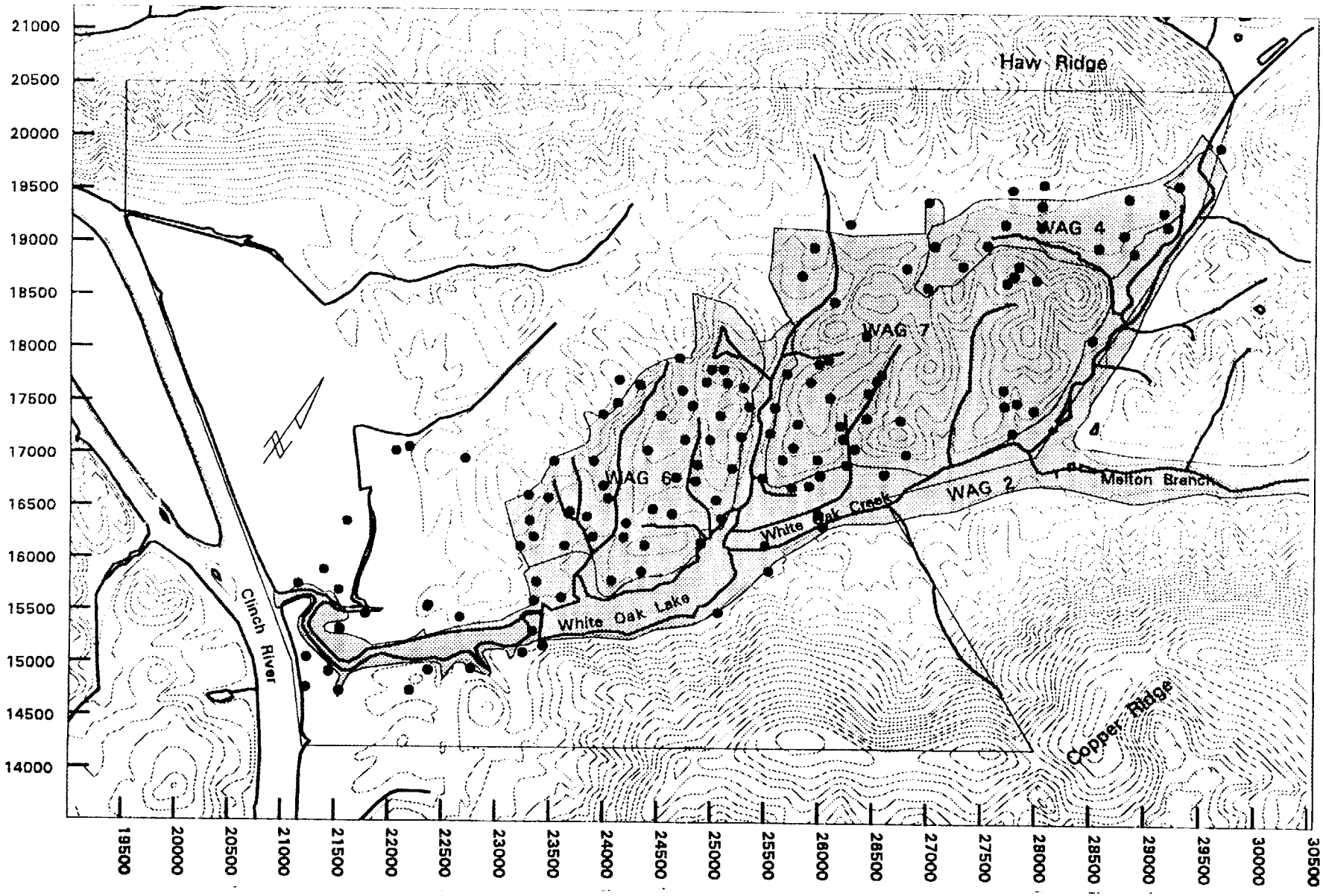

Figure 2. **Location of calibration piezometers (represented by dots) in the Western Melton Valley model area.** Also shown is the location of WAGs in the model area.

the preliminary estimate of head there provides an important data point for understanding flow around White Oak Lake, and thus was included in calibration. Both the OREIS and the HHMS data sets were averaged through seasonal variations over 3 years to provide an approximation of steady-state water levels.

Aside from water level measurements, fluxes obtained from surface water measuring stations during the dry season, which should represent groundwater baseflow, are also being compared with calculated fluxes. This serves as an additional check on how well the groundwater model simulates actual conditions in the field.

2.3 HYDRAULIC CONDUCTIVITIES

Hydraulic conductivity (K) patterns in the model area were examined for spatial trends using the public domain software Geo-EAS (Englund and Sparks 1991). The most extensive K data are from the WAG 6 area, and the following analysis describes only these data.

There were 120 K measurements from slug tests (Table 2) available from the approximately 75-acre area of WAG 6 (compiled by Tom Zondlo, Environmental Sciences Division, ORNL, April 1992, data file transfer). These data were separated into several subsets for analysis to remove geologic and possible measurement trends:

allk -- full file
bedr -- bedrock
reg -- regolith
mary -- maryville
nol -- nolichucky
deep -- greater than 100 ft

The bedr, mary, and nol files had five bedrock low-K HHMS piezometers removed because they created higher variances, thus more noise. In addition, they are not completed in fractured intervals, and thus belong to a different population. Essentially, the HHMS piezometers represent matrix K rather than an equivalent porous media K, as more typical for measurements. Since including matrix K measurements creates a strong measurement trend, no further analysis is reported for the allk file.

Variogram analysis to determine spatial correlation was conducted for reg, mary, and bedr. Nol and deep have insufficient data for analysis. The maximum correlated distance seems to be reached in less than 250 ft in all cases, and lags (modeler-selected correlation distances) of 20 to 25 ft produce large enough data groups for analysis. All models fitted a Gaussian variogram, which has a shape that is a bit flat at first, fairly flat slope up. The nugget (minimum) was around 1; the sill (where the correlation begins to level off) was between 2 and 3; and the range, the maximum correlation distance, was between 125 and 200 ft.

Table 2. Hydraulic conductivities measured in Waste Area Grouping 6

WELL #	NORTH	EAST	K CM/SEC	B/SCRN DEPTH	2/21/90 WATER LEVEL ELEV.	B/SCRN ELEV.
745	16067.8	23808.3	2.05E-04	60.2	753.98	693.98
832	17385.6	24096.7	1.70E-05	85.6	801.45	752.65
833	16056.9	23842.4	1.56E-04	30.7	752.34	722.04
835	15767.7	23951.8	2.43E-04	26.9	747.93	733.03
836	15748.2	24138.8	2.63E-04	28.2	748.42	735.12
838	16308.7	24934.8	1.10E-04	21.5	749.96	730.79
839	16308.8	24923.6	5.01E-04	56	749.56	695.56
840	16928.6	25251.7	4.75E-04	26.6	750.14	740.34
841	17206.3	25294.8	4.40E-06	56.3	757.69	709.74
842	17216.1	25298.4	8.82E-05	23.2	760.25	744.05
843	17597.1	25221.4	1.05E-04	19.3	781.93	762.13
844	17602.5	25228.6	3.68E-06	51.7	773.15	729.25
845	17108.2	24988.3	3.42E-04	39.9	788.83	767.43
846	18030.7	24803.5	2.76E-06	81	825.88	780.03
849	16781.8	24215.2	2.19E-04	32.6	779.78	755.08
851	16485	24058.2	1.09E-04	20	767.66	746.36
852	16346.9	23911.6	3.19E-04	21.5	763.35	746.05
853	16695.1	24047.5	6.03E-05	25.8	773.29	754.59
854	16711.9	23851.9	5.80E-04	27.3	775.68	754.18
855	16755.3	23427.7	4.48E-04	51.7	799.88	759.58
856	16764.4	23432.9	1.90E-05	81.2	800.47	728.97
857	16538	23106.3	3.06E-04	69.6	798.58	777.58
858	16542.1	23115.8	2.00E-06	106.1	796.32	741.12
859	16009.4	23246.2	5.50E-04	26.2	771.06	751.7
860	15996.6	23252.9	3.02E-04	61.5	771.24	715.64
636	17668.04	24326.17	2.20E-05	54	806.81	779.03
637	17715.14	24135.97	1.51E-06	66	814.65	793.42
638	17495.05	24119.35	5.10E-05	70	810.53	778.36
639	17395.38	24138.11	2.20E-04	62.5	798.29	773.41
640	17614.7	24719.55	8.35E-05	60	804.17	775.84
641	17383.49	23985.24	3.94E-05	60	825.73	783.79
642	16580.96	24035.55	2.78E-05	30	773.48	743.03
644	16748.86	24848.36	1.97E-05	17	771.84	759.3
645	17173.65	25274.6	1.50E-04	25	759.66	739.78
646	17550.78	25167.05	4.76E-06	39	772.51	746.18
651	16870.85	25190.67	1.27E-04	95	768.93	701.32
652	16159.68	24900	2.44E-05	90	749.57	680.16
653	15792.51	24070.4	2.44E-04	60	747.8	703.54
654	16618.16	24054.76	1.86E-04	90	775.07	685.14
655	17469.72	24815.3	3.36E-05	125	801.92	713.29
656	17923.92	24692.96	4.87E-05	120	813.97	727.59
739	15628.89	23604.03	1.74E-04	33	747.75	726.86
740	15778.95	23372.39	2.67E-05	24	756.39	743.3
741	15596.74	23352.05	2.78E-04	22	748.18	736.31
748	15891.1	25534.6	9.10E-05	22.5	752.2	736.29
749	16314.9	26038.6	1.07E-04	22.5	755.78	736.36
T-1	16398.76	23552.76	7.76E-05	9.1	772.43	765.4
T-5	16343.83	23695.66	1.55E-04	4.7	766.58	762.8
T-7	16299.72	23550.04	3.68E-05	9.4	769.76	761.3
T-10	16250.96	23401.11	1.45E-04	21.6	776.21	760.8
T-17	16199.86	23550.51	4.58E-04	11.3	766.11	755.5

Table 2. (Continued)

WELL #	NORTH	EAST	K CM/SEC	B/SCRN DEPTH	2/21/90 WATER LEVEL ELEV.	B/SCRN ELEV.
T-18	16201.27	23653.42	1.61E-04	7.3	761.02	755.2
T-20	16200.98	23750.45	1.44E-04	10.8	759.86	750.3
T-22	16137.52	23405.93	4.59E-05	16	773.11	761.8
T-27	16098.86	23253.89	9.88E-05	19.3	773.54	766.1
T-36	15998.81	23455.12	1.45E-04	16.5	763.96	748.6
HHMS-4A	16144.55	24609.77	1.80E-09	400	646.79	390.37
HHMS-4B	16148.2	24688.37	3.40E-05	215.28	756.63	572.5
HHMS-4C	16170.59	24676.08	3.00E-04	61.5	757.56	726.36
HHMS-5B	15827.63	24595.29	4.70E-06	219.48	752.48	546.95
HHMS-5C	15833.46	24561.12	5.80E-05	63	747.91	703.79
HHMS-6A	15305.95	24764.04	4.20E-09	400	730.39	362.09
HHMS-6B	15289.25	24745.16	4.20E-06	295	747.56	467.27
HHMS-6C	15268.72	24732.51	6.60E-05	178	754.65	584.47
HHMS-7A	17540.65	24512.09	2.30E-08	400	789.59	408.54
HHMS-7B	17518.9	24509.4	7.60E-07	295	791.93	513.64
HHMS-7C	17498.37	24506.56	7.30E-07	178	800.97	630.76
HHMS-8A	16862.02	24694.84	1.90E-09	400	637.33	386.06
HHMS-8B	16810.7	24697.05	1.70E-08	197	776.44	586.53
HHMS-8C	16782.51	24668.21	5.60E-06	79	778.88	707.09
ETF-5	16732.5	23665.3	3.02E-04	30.25	783.19	764.22
ETF-6	16724.1	23651	3.94E-04	30.09	783.05	764.22
ETF-7	16723.2	23633.6	1.97E-04	30.41	783.4	763.55
ETF-8	16729.2	23618.6	3.13E-04	29.76	784.15	763.18
ETF-9	16745.3	23610.3	4.99E-05	30.91	788.17	763.11
ETF-11	16773	23702.6	2.44E-04	49.58	780.57	742.01
ETF-12	16737.9	23584.4	4.05E-04	50.1	785.07	740.05
ETF-13	16872	23596.3	1.74E-05	250.73	793.11	558.49
ETF-14	16849.2	23618.5	2.31E-05	94.59	795.41	710.37
ETF-15	16841.4	23603.5	6.60E-06	46.75	794.59	758.83
ETF-16	16841.4	23614.1	2.89E-05	244.5	794.24	560.47
ETF-17	16782.9	23606.4	9.61E-06	18.73	789.59	780.45
ETF-20	16769.5	23606.7	2.31E-04	21.82		774.94
ETF-22	16788	23641.2	4.24E-05	22.51	785.58	777.61
ETF-25	16773.9	23637.9	7.62E-05	21.59	784.86	776.95
ETF-27	16745.5	23616.4	2.19E-05	20.41	784.75	774.43
ETF-29	16769.4	23651.4	2.19E-05	20.74	783.94	777.25
ETF-36	16749.1	23658.6	1.52E-05	21.16	784.11	775.27
ETF-39	16735.8	23654.9	4.27E-05	22.18	783.8	773.43
ETF-40	16743.6	23671.4	5.54E-05	20.67	783.31	774.37
368	17348	25155	1.85E-03	39	790.77	780.5
371	16393	25090	5.65E-05	30	746.73	735.4
374	17462	25346	9.85E-05	31	767.85	750.28
376	16584	23479	7.73E-04	35	787.94	771.46
379	16156	23206	1.06E-04	37	775.11	755.13
380	15977	23320	4.27E-04	31	767.54	741.55
381	16248	24266	6.00E-05	35.35	759.24	742.24
382	15814	24025	6.00E-05	21	748.05	742.34
383	16165	24895	7.77E-05	33	747.78	736.38

The spatial correlation can be used to krige the K data and produce a spatial distribution of K based on the point measurements. However, the cross-validation analysis, which compares observed and kriged data, shows a very poor match. For both the regolith and the bedrock, the kriged standard deviation is about the same as the population standard deviation, indicating that the errors introduced by kriging are about the same as the errors introduced by using a mean value. Two explanations for the poor cross validation can be suggested: (1) the data are very heterogeneous; (2) the sill occurs at a much shorter distance than the typical distance between measuring points, so very few neighboring data points can be used for estimation.

Because this analysis did not clearly show a benefit from horizontally distributed K patterns, a uniform K pattern was used in different model layers (Sect. 4.1).

2.4. PRECIPITATION AND RECHARGE

The average annual rainfall measured in the Oak Ridge Reservation from 1954 through 1983 is approximately 52 in. (Moore 1988). Recharge to groundwater has been estimated to be between 0.5 to 2.75 in. per year (Solomon et al. 1992, pp. 3-16). Recharge and discharge are difficult to estimate because of uncertainties in the amount of stream discharge that originates from wastewater generated by ORNL plant operations. However, recharge to the groundwater zone is significantly less than rainfall.

3. DEVELOPMENT AND CALIBRATION OF GROUNDWATER FLOW MODEL

3.1 MODEL CONSTRUCTION

The construction of the Melton Valley groundwater model was facilitated by the use of I-Deas, a workstation-based, finite-element grid generation and analysis program (Structural Dynamics Research Corporation). The user defines the geometry of the domain and specifies desired finite-element mesh characteristics, then the preprocessor discretizes the domain into elements and associated nodes. Locations of boundary conditions for streams were also defined in I-Deas, although specific values for heads or variable fluxes were assigned in an external program (described below). Without the use of I-Deas, it would have been extremely tedious to develop a three-dimensional, finite-element grid as complex as the Melton Valley groundwater flow model.

Although I-Deas is capable of discretizing three-dimensional domains, it was only used to generate a finite-element grid on the top surface of the model (Fig. 3). A separate preprocessing subroutine was written, which took as input the surface discretization produced by I-Deas and generated the full three-dimensional domain by regenerating the remaining nodes by layers (Fig. 4). This "layered" approach was taken because it was not feasible to develop the full 3-D model with more than 40,000 nodes on a workstation with a limited amount of disk storage. The resulting surface grid has 4624 surface elements with ~100-ft-long sides. The full 3-D model derived from the surface grid generated by I-Deas has 41,616 nodes.

Topographic information for the model region was obtained from OREIS and was accessed using the ARC/INFO Geographic Information System. The definition of the topographic surface on I-Deas consisted of the following steps: (1) locations of the nodes were written from I-Deas to an ASCII file; (2) 20-ft contour lines in ARC/INFO were assigned values for topography; (3) node locations, stream locations, and elevations were read into ARC/NFO; and (4) an interpolation program in ARC/INFO generated the elevation at all nodes. This elevation file was translated into the P-FEM input files.

After the I-Deas grid and ARC/INFO elevation file are generated, a separate program (FEMPREC.C) is used to translate the grid information to the format required by P-FEM. FEMPREC.C prompts the user for number of nodes in the surface layer, number and thickness of layers, material properties (hydraulic conductivity), fluxes (recharge rate), and an elevation file (Fig. 5). Then it creates the separate input files for each of the possible 17 datasets used by FEMWATER (Yeh 1987). A separate program, FEMGRID.F, is used to split the model region into subregions, which are each assigned a different processor on the supercomputer. Ideas could also be used to visualize output by converting P-FEM storage files to I-Deas format using another program, FEMPOST.C (Fig. 6).

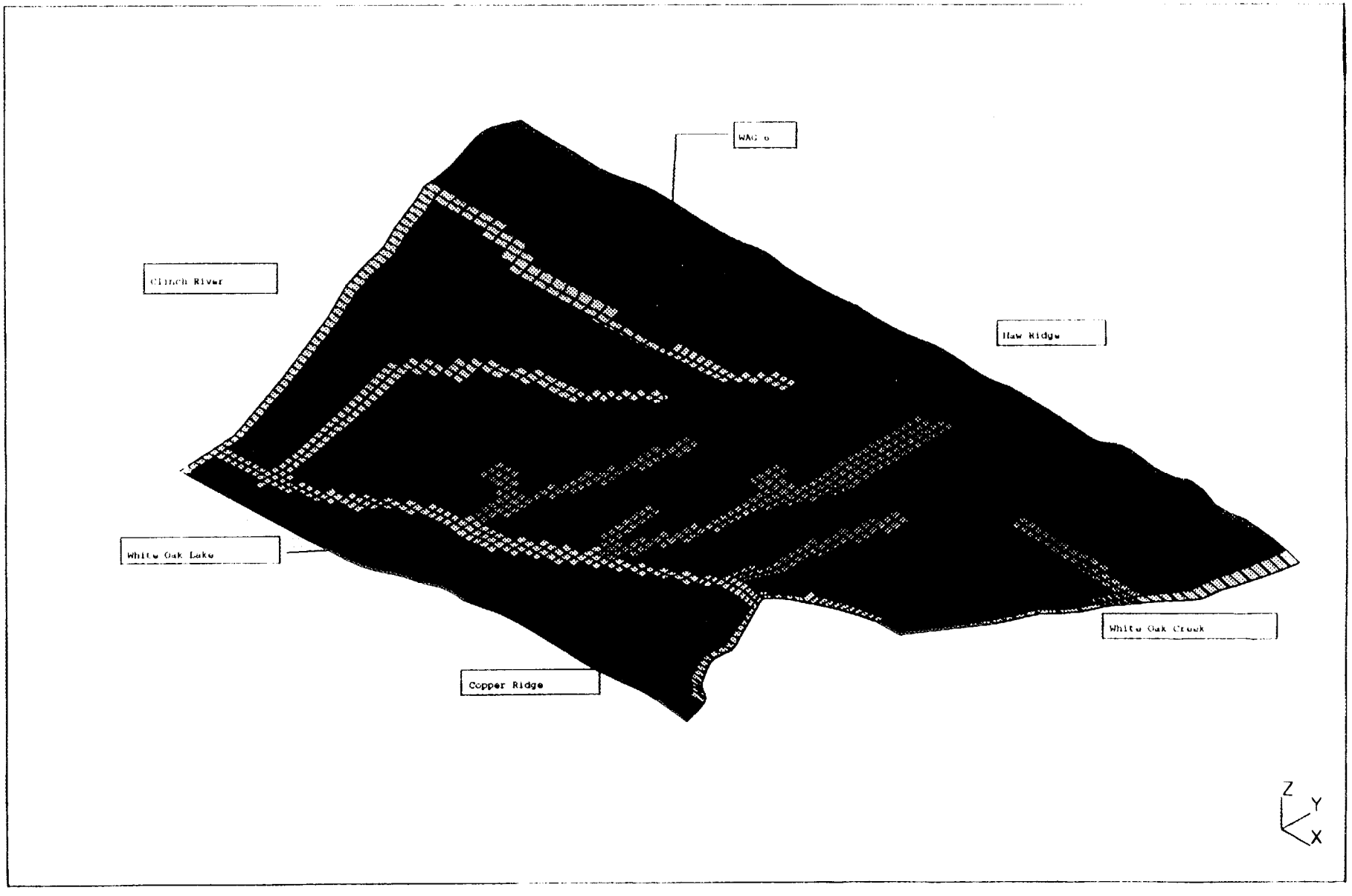

Figure 3. Finite-element surface grid of the topographic surface of the model, showing boundary conditions. Light-gray are specified head elements; dark-gray are ephemeral streams modeled as variable recharge or head boundaries.

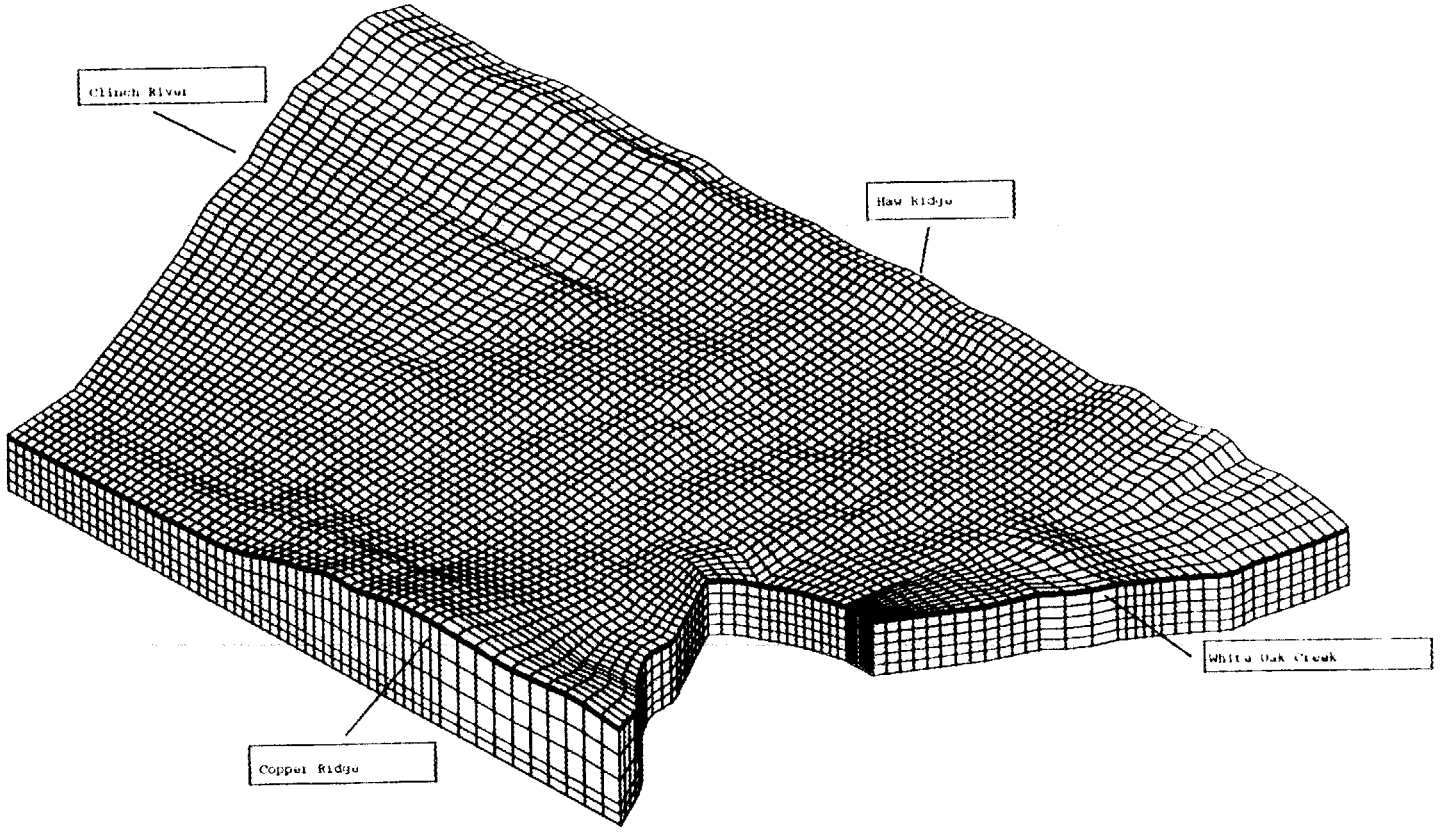

Figure 4. **Full three-dimensional, finite-element grid, produced by the pre-processing routine from the surface grid generated by I-Deas.**

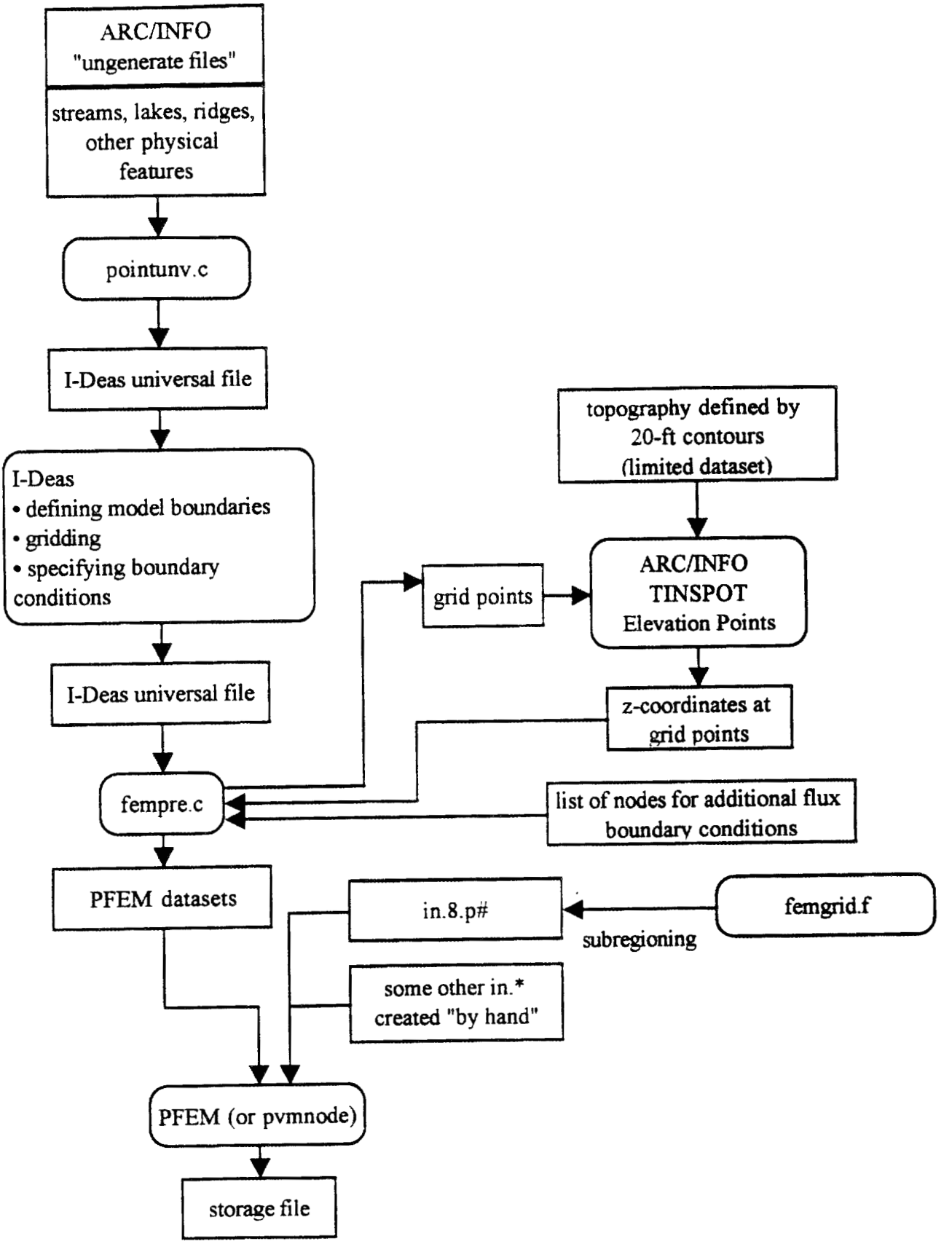

Figure 5. Diagram of the pre-processing program used to generate model input. File names are in boxes, program names in ovals.

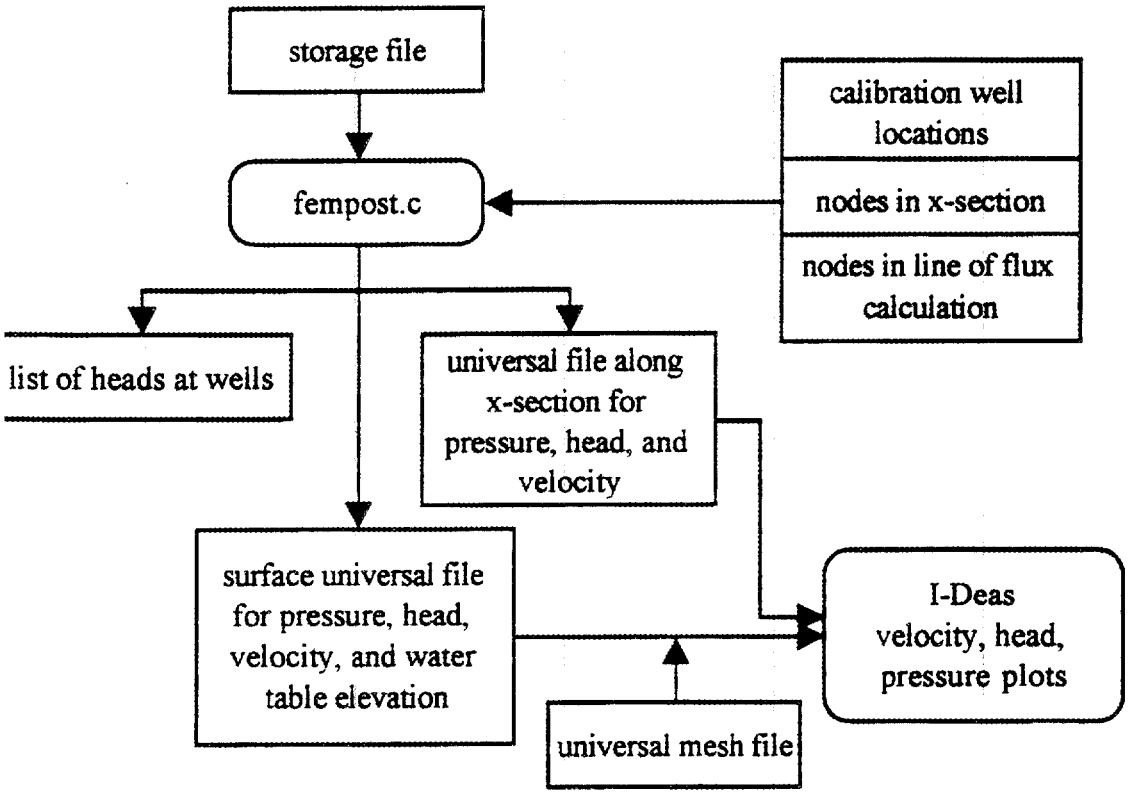

Figure 6. Diagram of the post-processing program used to visualize model output. File names are in boxes, program names in ovals.

3.2 BOUNDARY CONDITIONS

All of the vertical sides and the bottom of the 3-D Melton Valley groundwater flow model were initially specified as impermeable boundaries. This assumption implies that (1) Haw and Copper ridges are groundwater divides, and (2) there is no groundwater underflow beneath the Clinch River and the north trending branch of White Oak Creek. There is currently very little evidence that would support the validity of these assumptions. As mentioned previously, however, WAG 6 is distant from these boundaries, and calculations made within the region of interest will probably not be significantly affected by the assumptions made at the boundaries. Water-level data from HHMS-6A was used to calibrate to some underflow beneath Copper Ridge, modifying this from a no-flow boundary.

Lakes and perennial streams (light-gray elements in Fig. 3) were modeled as specified head nodes, whereas ephemeral streams (dark-gray elements in Fig. 3) were specified as rainfall-seepage nodes. At the specified head nodes; total heads were set to the elevations of the nodes, i.e., pressure head was set to 0. The rainfall-seepage nodes can be either a specified head node or a specified flux node, depending on the maximum amount of ponding allowed (pressure head at the node =< maximum ponding depth) or the maximum flux expected (flux at node =< maximum recharge rate). The maximum ponding depth for all the seepage nodes was set to 0 since the depths of the streams and lakes are small relative to the depth of the entire model.

Except for the elements that coincide with streams and lakes, all of the element faces on the top surface of the model are specified flux (Cauchy) elements, where the specified flux was equal to the amount of recharge to the groundwater. The recharge value varied over the model domain (Sect. # 4.1).

3.3 MATERIAL PROPERTIES: LAYERING

The Melton Valley groundwater model was constructed with three layers: the regolith, shallow bedrock, and deep bedrock (Fig. 7). The hydraulic conductivity of these three layers decreases with depth. This conceptualization of the groundwater flow system follows that of Tucci (1991) and Solomon et al. (1992). The stormflow zone has no equivalent in the conceptualization of the Melton Valley groundwater model. Although this flow zone is known to carry a large percentage of the water flux, its inclusion was considered beyond the scope of the steady-state groundwater model because it is a transient flow zone that only becomes inundated during storm events.

Each layer in the Melton Valley groundwater model was assumed to be homogeneous. Because there is some evidence of anisotropy within the groundwater flow system (Solomon et al. 1992), both anisotropic and isotropic hydraulic conductivities in the x:z and x:y directions were modeled. However, anisotropic values selected were uniform throughout the model domain, and x:z anisotropy was perpendicular to the land surface, although angled bedding is also an option.

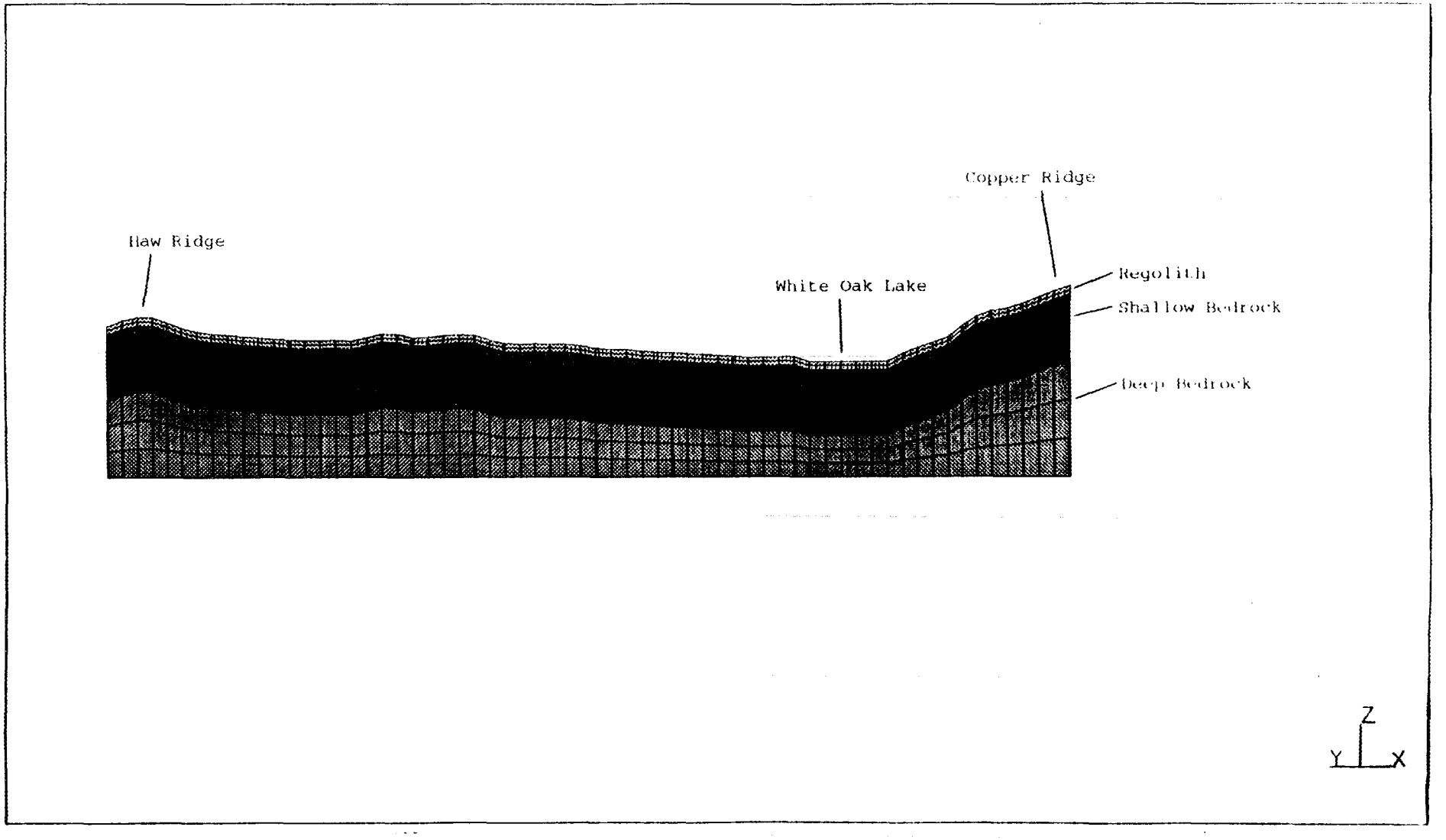

Figure 7. Cross section showing hydraulic conductivity layers in the model.

In all of the analyses described in this report, hydraulic conductivities of the intermediate and deep bedrock layers were held constant at 1×10^7 and 1×10^9 ft/s, respectively. The interface between the deep and shallow bedrock layers was also kept at 400 ft ASL for all of the runs. The interface between regolith and shallow bedrock was made to follow the surface topography, resulting in a constant regolith thickness of 40 ft.

3.4 CALIBRATION PROCEDURES

The model runs were focused on calibrating the groundwater model by selecting hydraulic conductivities (including anisotropy ratios), recharge rates, and underflow fluxes (beneath Copper Ridge) that will minimize the difference between measured and modeled water levels. Calibration of the Melton Valley groundwater model consisted of varying the recharge and the hydraulic conductivity of the regolith layer to match water levels measured in piezometers included in the calibration data sets. Further checks on the calibration included comparing measured and modeled stream fluxes at four gaging stations near or in WAG 6 and plotting the pressure heads to map the depth of the water table zone--zero pressure head should occur at the surface only where there are surface water bodies. The pressure head should be negative elsewhere at the land surface, indicating the presence of an unsaturated zone.

4. RESULTS

4.1 SHALLOW PIEZOMETER CALIBRATION AND COMPARISON TO DEEP PIEZOMETER DATA

A measure of the degree to which the computed water levels match the measured water levels is given by the root mean square error (RMSE), which is defined as follows:

$$RMSE = \sqrt{\frac{\sum_{N_W} (MWT_i - CWT_i)^2}{N_w}}$$

where MWT_i and CWT_i are the measured and computed water levels at piezometer i, and N_w is the number of piezometers in the calibration set.

The base case calibrated model has an RMSE (excluding the HHMS piezometers) of 11.2 ft. The HHMS piezometers have a similar RMSE (11.5 ft), but vertical flow trends are not always matched. Calibration of the deep system through adjustment of the groundwater divides, variation in hydraulic conductivity, and anisotropy is not yet complete. Further improvements of the RMSE could be obtained, but calibration efforts are now focused on a different model grid (Sect. 5).

The calibrated model characteristics are:

1. Layer properties -- Thickness and K_x
   Regolith: Thickness = 40 ft, K = 4×10^{-6} ft/s
   Shallow Bedrock: Thickness = 310 ft, K = 1×10^{-7} ft/s
   Deep Bedrock: Bottom elevation at 200 ft, variable thickness,
   K = 1×10^{-9} ft/s
   X:Z Anisotropy: 1:5

2. Recharge patterns
   Recharge over area north of White Oak Lake + Creek = 6×10^{-9} ft/s (3.0 in./year)
   Recharge over area south of White Oak Lake + Creek = 0 ft/s
   Recharge over White Oak Lake and tributaries = 0 ft/s

3. Underflow patterns
   Underflow beneath Copper Ridge in Shallow Bedrock = 1×10^{-9} ft/s
   Underflow beneath Copper Ridge in Deep Bedrock = 1×10^{-10} ft/s

A comparison between measured and modeled water levels in the non-HHMS piezometers (Fig. 8) shows a better match at lower head values (typically lower elevations). This suggests that the simple, uniform recharge pattern is not adequate. The next step is to assign different recharge values for hill tops, hill slopes, and valleys in greater detail than the patterns described above. Alternately, hydraulic conductivity could be varied, but recharge should be adjusted first because the range in values is much smaller than the range in K. A map of error in the calibration (Fig. 9) shows some clustering of error locations, further indicating smaller scale trends in recharge or hydraulic conductivity that have not yet been captured in the relatively homogeneous model.

A comparison between measured and modeled water levels in HHMS piezometers (including 1 through 9 only) indicates vertical components of flow have not been created by the selected boundary conditions and hydraulic conductivities. Model runs with a vertical to horizontal anisotropy ratio of 0.2 indicate a better match to the deep system, and further testing of ratios and rotation of the anisotropy axis is under way. Anisotropy and hydraulic conductivity alone cannot reduce heads where they are overestimated by the model, and the deep system is not sensitive to recharge. Thus, we altered the Copper Ridge boundary condition as well.

The use of underflow beneath Copper Ridge in shallow and deep bedrock improves calibration, but it actually has little influence on contaminant pathways. Rather, it is important to establish this boundary to better construct small-scale models, estimate groundwater discharge to White Oak Lake, and calibrate regional parameters such as anisotropy. In fact, the use of a discharge boundary in shallow bedrock here can be considered the equivalent of moving the Copper Ridge boundary horizontally without having to go through the tedious process of regridding a 40,000-node problem domain. As shown in Fig. 10, all of the water discharge beneath Copper Ridge comes from either (1) shallow bedrock south of White Oak Lake, which contains no known waste areas, or (2) the deep groundwater system with extremely low flow rates, nonpotable water, and little or no contact with sources. One possible contact with deep waste would be hydrofracture contamination, but the model is not yet calibrated in that area; underflow may not be a concern.

The values selected for underflow are based on the location of the groundwater divide in shallow bedrock (where flow lines separate into White Oak Lake discharge and discharge to the south of Copper Ridge), comparison to observed heads, and the overall pressure distribution. It has been observed that specifying very high underflow beneath Copper Ridge results in unreasonable pressure and velocity distributions. For example, a flux value within the deep bedrock layer that is on the same order of magnitude as the conductivity of the deep bedrock (1×10^{-9} ft/s) produced dewatering of the rock (i.e., negative pressures). In addition, higher underflow values within the shallow bedrock caused the groundwater divide to be too close to White Oak Lake. Note that underflow does not appear to significantly affect the heads and flow rates north of White Oak lake.

Another measure of calibration is groundwater discharge (Fig. 11). The total dry season flow, which should represent groundwater base flow, and modeled flux agree within 10%. West Seep, which has the highest flux value, shows the poorest match, and

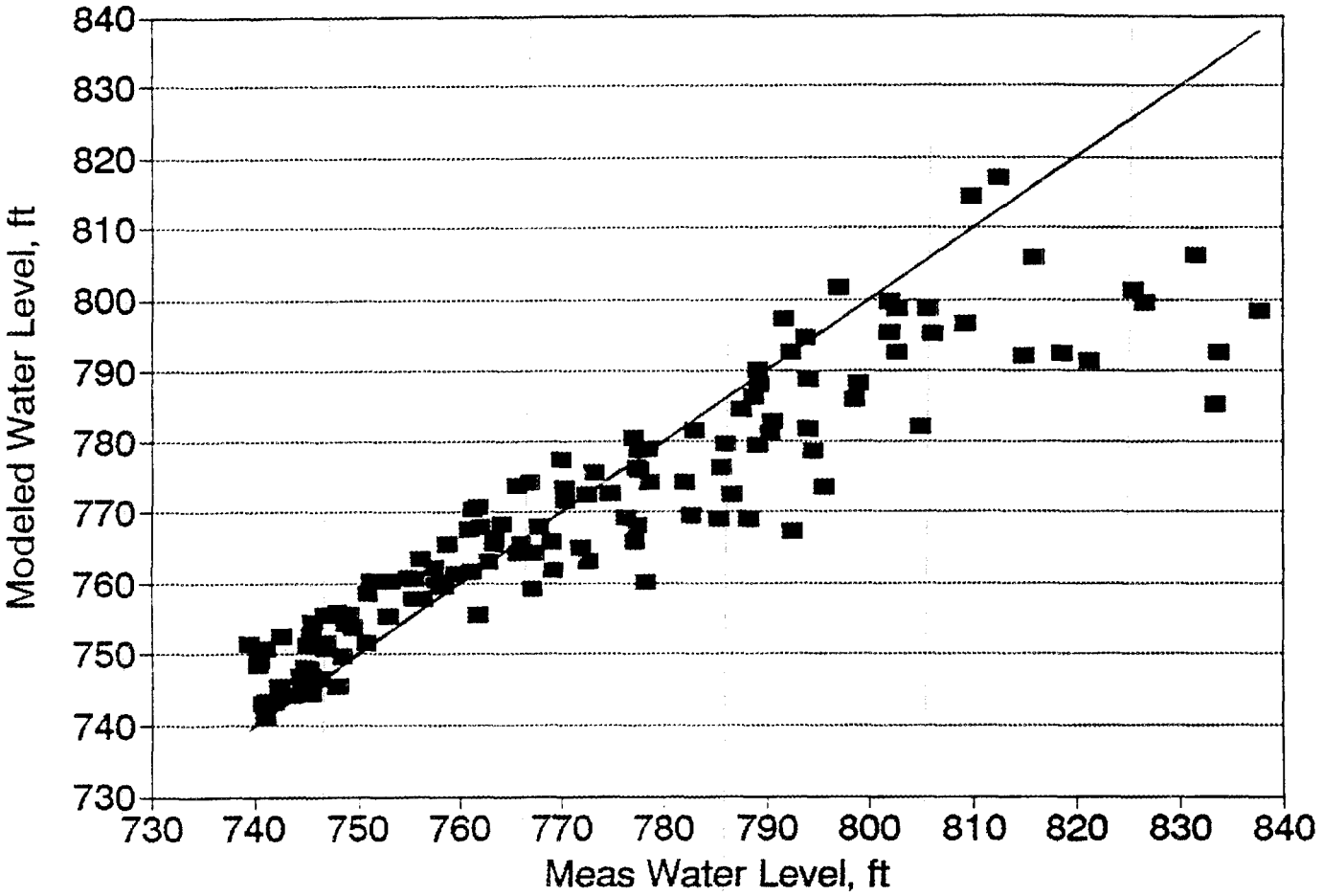

Figure 8. **Modeled water level versus measured water level in the shallow calibration data set.**

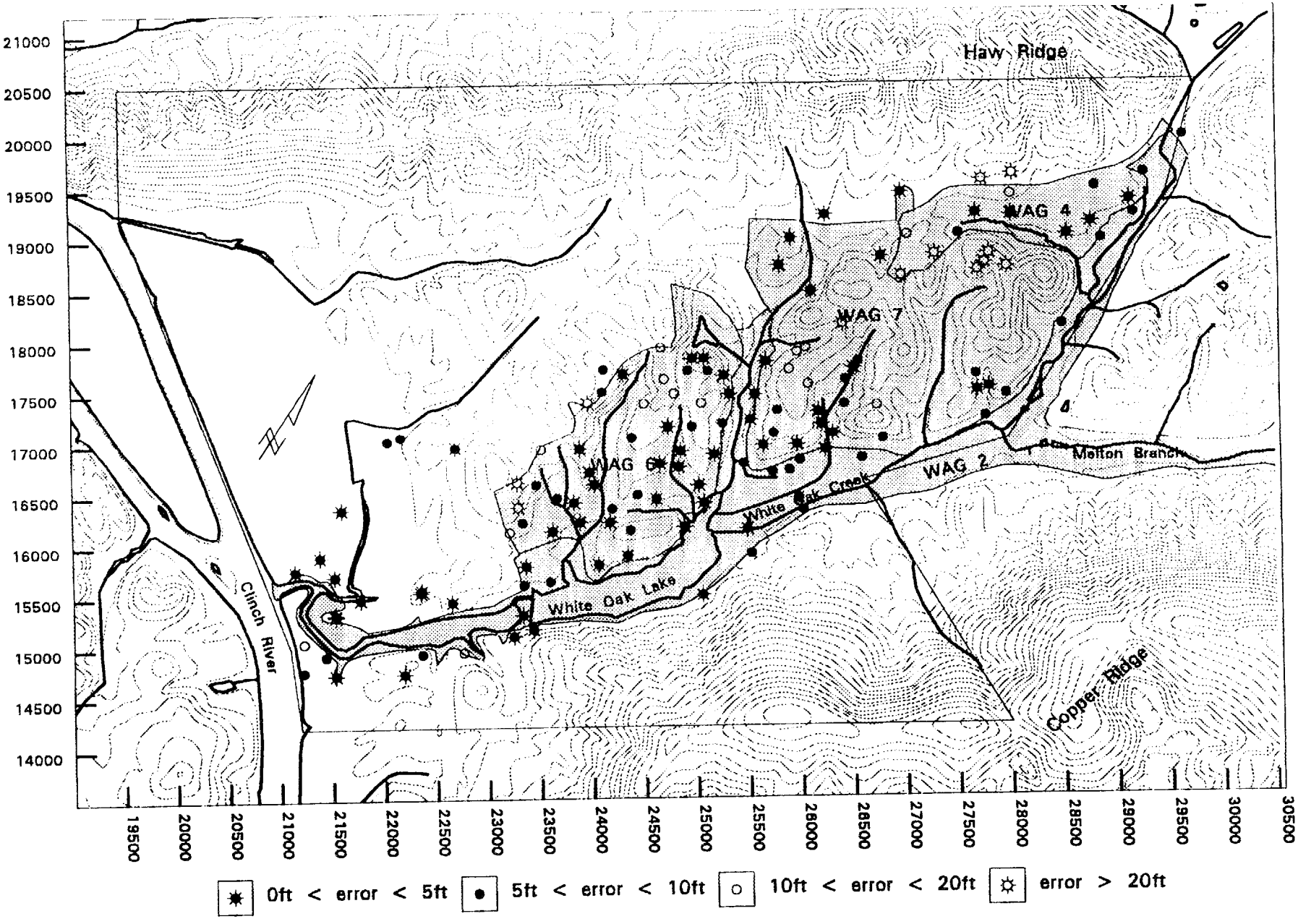

Figure 9. Map of degree of model error in piezometers selected for calibration. Legend symbol indicates absolute residual error.

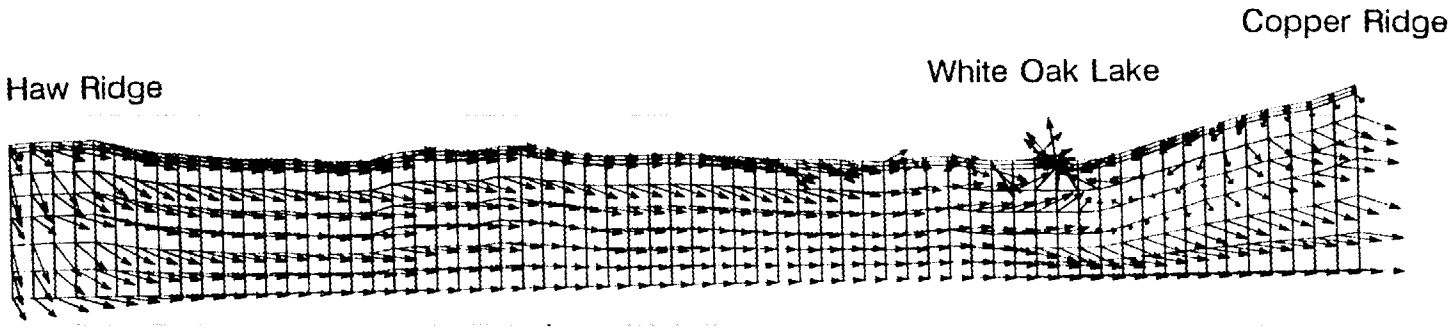

Figure 10. North-south cross section through White Oak Lake showing flow vectors.

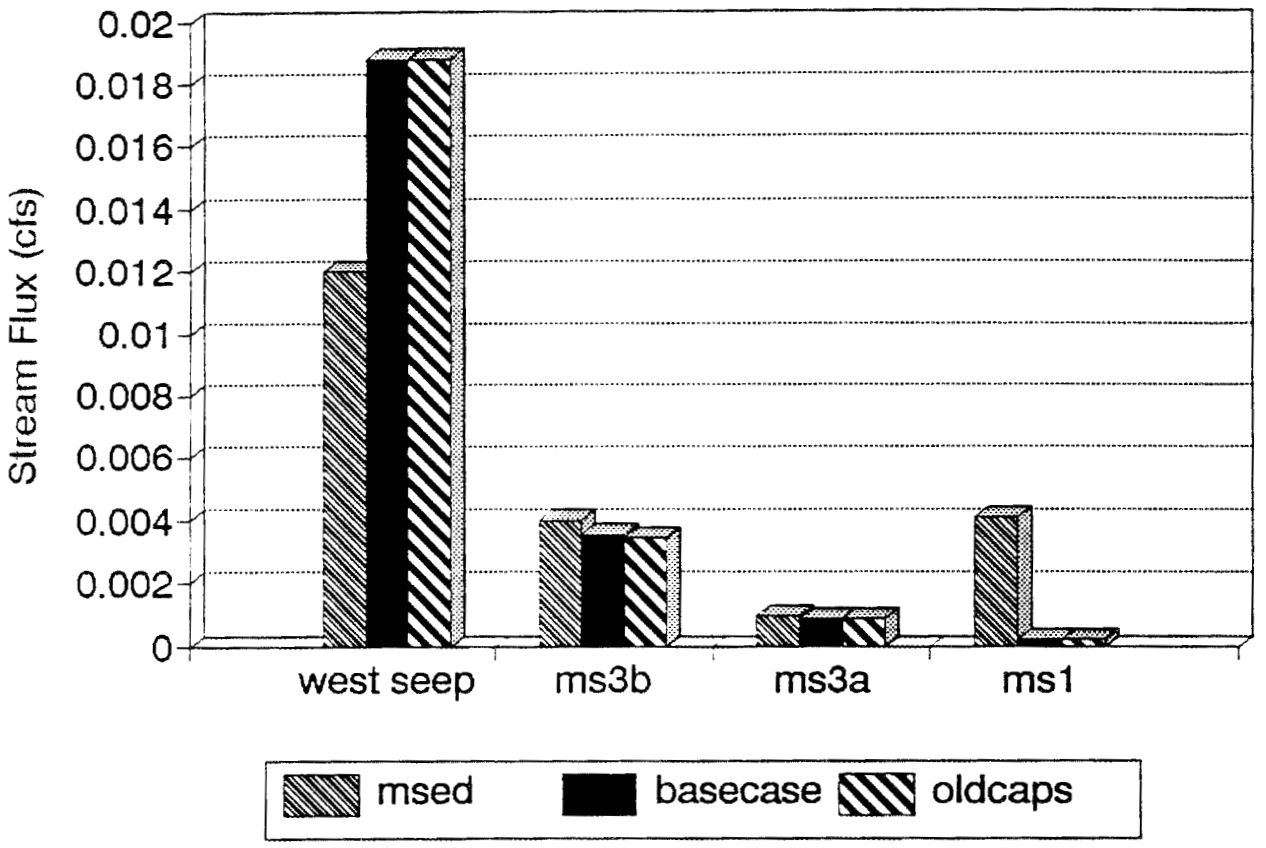

Figure 11. Bar chart of measured and modeled stream fluxes for 4 gaged stations in WAG 6. Measured data from MS1, MS3A, MS3B from Donna Pridmore, Environmental Sciences Division, personal communication, February 1994. Measured data from West Seep from Borders et al., 1993.

more calibration should be done here (e.g., x:y anisotropy or locally increased K). These stream fluxes are low season values (typically in September) reported over just a year or two (data sources on Fig. 11), but the dynamic range between wet and dry seasons suggests that the model captures the low fluxes, and the shallow model calibration is reasonably good.

4.2 SELECTED ALTERNATE MODELS

A formal sensitivity analysis of model parameters has not been conducted; this work is planned for the new model grid. However, selected alternate models were run in the course of calibration, which can provide an indication of the importance of some of the parameters selected. These alternate models include:

- no underflow beneath Copper Ridge;
- isotropic hydraulic conductivity in x, y, and z;
- anisotropic hydraulic conductivity with x:y of 2:1;
- uniform recharge of 4×10^{-9} ft/s; and
- flat bedrock/regolith interface (instead of topographically dependent).

Each of these cases was run using the parameters indicated in Sect. 4.1, except for varying one parameter. This method will not give a true sensitivity to a parameter, but nonetheless indicated which parameters improve calibration and which do not. The results of these runs are summarized by examining two output values (Table 3): the RMSE of

	RMSE	Westseep cubic ft/s
base case	11.2	0.0278
x:y anisotropy	10.3	0.0204
isotropic	12.1	0.025
no underflow	11.2	0.0279
uniform R	12.4	0.0213
caps	11.2	0.0276
measured		0.012

Table 3. Comparison of root mean square error (RMSE) and flux to West Seep for several model runs

heads and discharge to the West Seep (primary discharge of WAG 6). There was an improvement in calibration by using an x:y anisotropy of 2:1. Anisotropy along strike has typically been hypothesized owing to increased flow along fracture intersections. The model construction of the flat regolith boundary would not converge, but an earlier version of this model that converged showed significantly worse RMSE. A flat bedrock interface is a physically unreasonable model construction, so no further refinement was conducted to obtain model output. All of the other parameter changes resulted in worse calibration of both RMSE and West Seep discharge. The errors did not tend to be focused on a particular region, as roughly indicated by plotting results from some individual piezometers located across the model area (Figs. 12 and 13). An exception to this is that HHMS-6A showed a poor calibration when underflow beneath Copper Ridge was eliminated, and this piezometer was the main calibration point for this underflow.

4.3 EFFECTS OF CAPS IN WAG 6

One of the applications for the Melton Valley groundwater model is the prediction of water level drops caused by the proposed placement of caps over trenches in the WAG 6 burial grounds. Proponents of this approach to remediating WAG 6 have claimed that the caps will lower the water table and will thus reduce contact between the waste in the burial trenches and the groundwater. This hypothesis was tested using the Melton Valley groundwater model.

Two scenarios were compared: bare ground and existing caps (CAP1). The effect of the caps was modeled by removing recharge on surfaces within the cap boundaries (Fig. 14). This assumes that the caps are drained and precipitation on caps is channeled to streams. It also assumes that increased discharge in streams does not create conditions where the streams become infiltration areas (boundary conditions are not altered).

CAP1 shows an average 0.08-ft decline with a maximum of 0.63 ft. These declines have a similar magnitude to overall mean model error, so further improvement in model calibration is needed to predict capped conditions accurately. The measured decline in water levels since capping is 0 to 1 ft (SAIC 1993a).

Another evaluation of cap effectiveness is to note changes in stream fluxes with and without caps (Fig. 11). If the cap creates a significant change in groundwater flow, fluxes to streams should decrease after capping. These fluxes were calculated by modifying P-FEM to print nodal fluxes at boundaries, not just total flux in and out. Fluxes decreased after capping, but changed less than 0.5%, indicating limited response to capping (Fig. 11). No decline was seen in West Seep, which has the largest off-WAG flux value. Vector plots of pre- and post-capping conditions indicate no discernable changes in flow paths due to capping (Fig. 14).

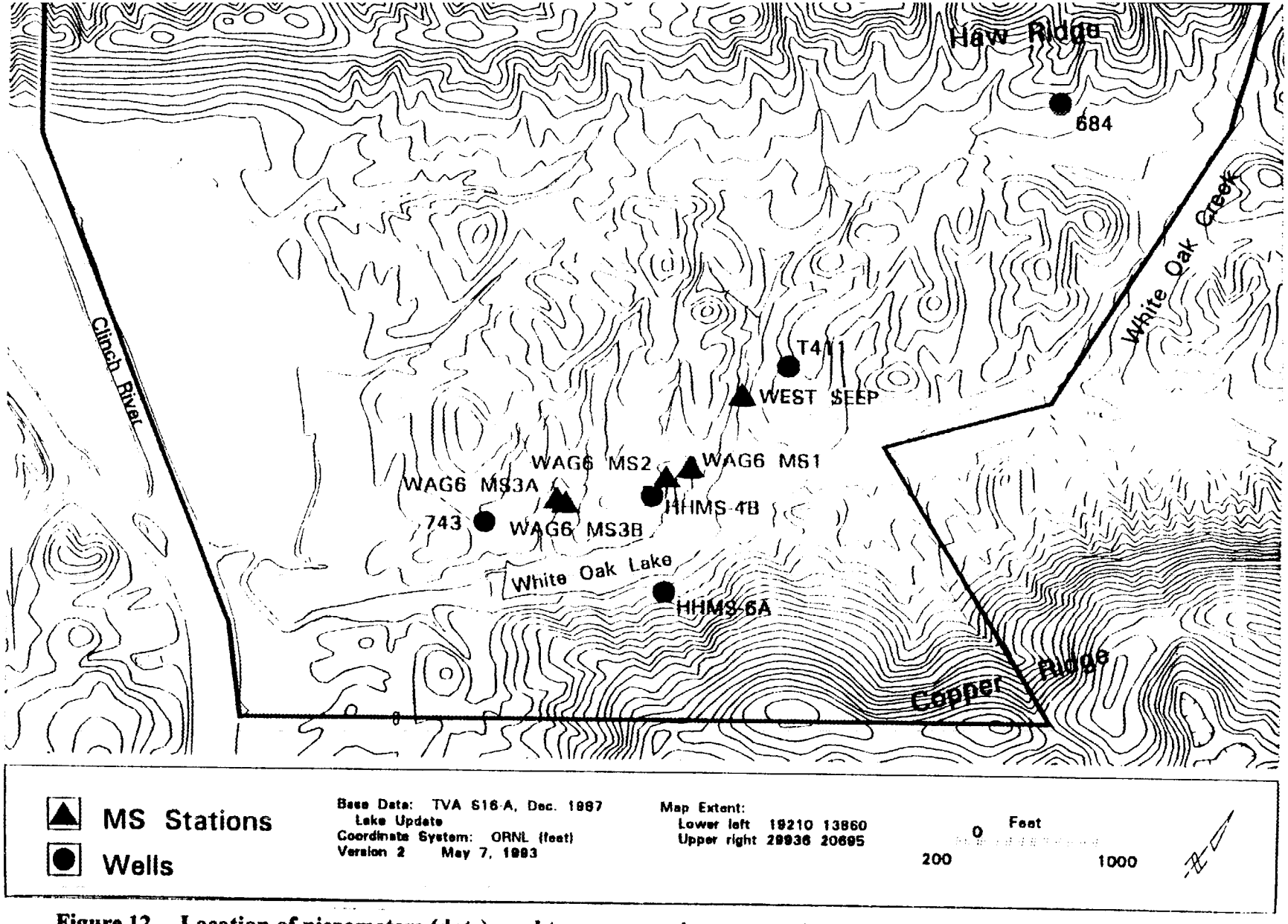

Figure 12. Location of piezometers (dots) used to compare alternate models and stream gages (triangles) used in Fig. 11.

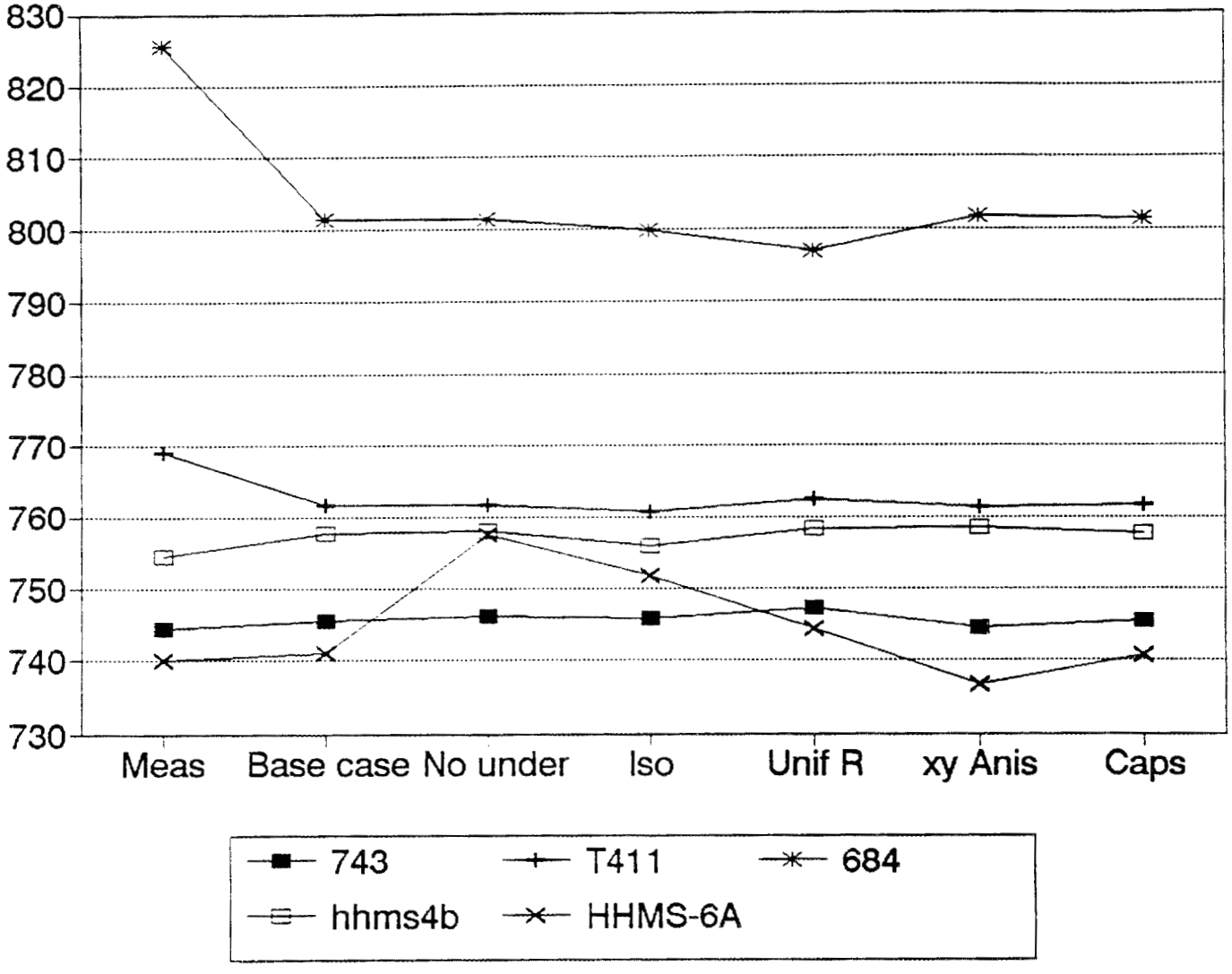

Figure 13. Head values in selected piezometers for alternate models.

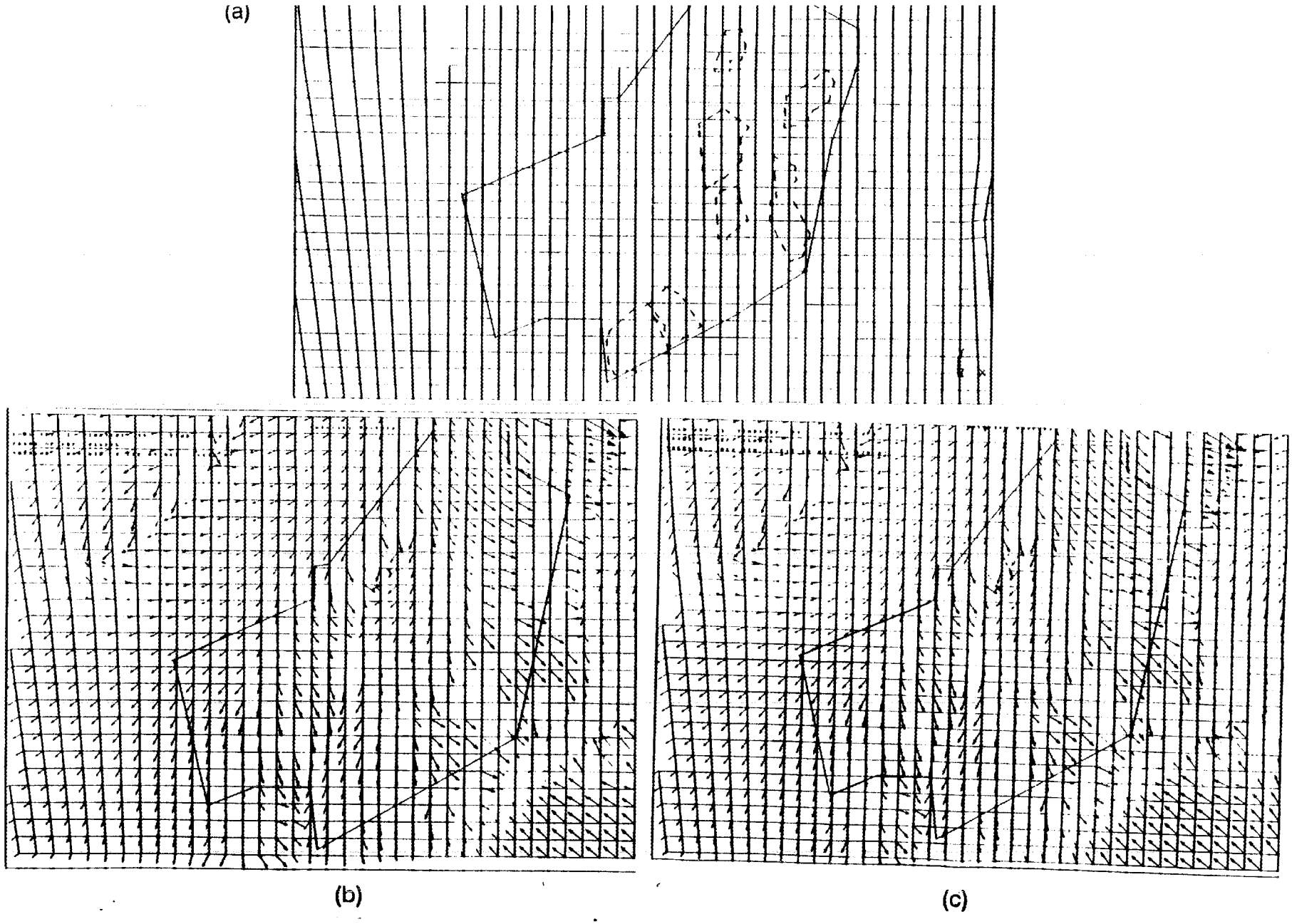

Figure 14. Comparison of capped and bare-ground models: (a) location of caps; (b) vector plots for bare-ground, and (c) vector plots for capped conditions.

4.4 COMPARISON OF LARGE- AND SMALL-SCALE MODELS OF WAG 6

This section provides a comparison of selected results from large- and small-scale models of WAG 6 and provides information on model values to use for estimating groundwater flux off WAG 6. A small model (called WAG 6) with boundaries close to the physical WAG 6 boundaries was developed by Environmental Consulting Engineers, Inc., to answer design questions for the WAG 6 Performance Assessment (EBASCO 1993; Gamliel et al. 1993). The large model of Western Melton Valley (called Western Melton Valley or MV model), with boundaries from Haw Ridge to Copper Ridge and encompassing WAG 6, was viewed as an additional modeling tool, but it was not known if it could be used to answer the same set of questions. While this uncertainty has not been completely resolved, the model comparison of two independently constructed models is useful in improving model conceptualization and calibration. A key question that needed to be answered for risk assessment of WAG 6 contaminants was what value of groundwater fluxes to use in estimating contaminant fluxes, and the work described here was geared to providing a recommendation for that work.

In addition to the smaller model domain, the vertical discretization of hydraulic conductivity zones is finer and shallower for the WAG 6 model. A comparison of parameter values shows similar hydraulic conductivity values chosen for each model, with a factor of 2 to 3 higher recharge for the WAG 6 model.

Results from the WAG 6 portion of the two models were quite similar. Calculations of residual error using the same set of piezometers were 4 for the WAG 6 model and 4.7 for the anisotropic MV model. A map of errors for each model indicates that essentially the same set of piezometers contributes the main portion of the model error. Vector plots and contour plots are similar except near the WAG 6 model boundaries.

Groundwater fluxes for risk assessment were calculated along five separate sections (Fig. 15, SAIC 1993b) representing the assumed drainage areas of WAG 6 not captured by surface water monitoring. Fluxes were calculated by three methods: (1) estimates of flux through the recharge area for the different catchments (R. B. Clapp, Environmental Sciences Division, ORNL, personal communication; SAIC 1993b); (2) the WAG 6 model (data from Environmental Consulting Engineers, Inc., November 1993); and (3) the MV model.

The fluxes from all three methods agree within an order of magnitude (Table 4). Sections 1 and 2 match closely. Sections 3 and 5 are nearly an order of magnitude different, but absolute values are lower than the other sections, so the error in total flux becomes small.

Section 4 (Fig. 15) is an exception to the above trend. The Clapp calculation and the MV model agree within a factor of 3, but the WAG 6 model value is 9 times larger than the Clapp model and 3 times larger than the MV model. Because this section seems to provide a major contribution to contaminant flux off WAG 6 because of high groundwater contaminant concentrations as well as high groundwater fluxes, it is particularly important to evaluate the reasonableness of the different methods of calculating flux for this section.

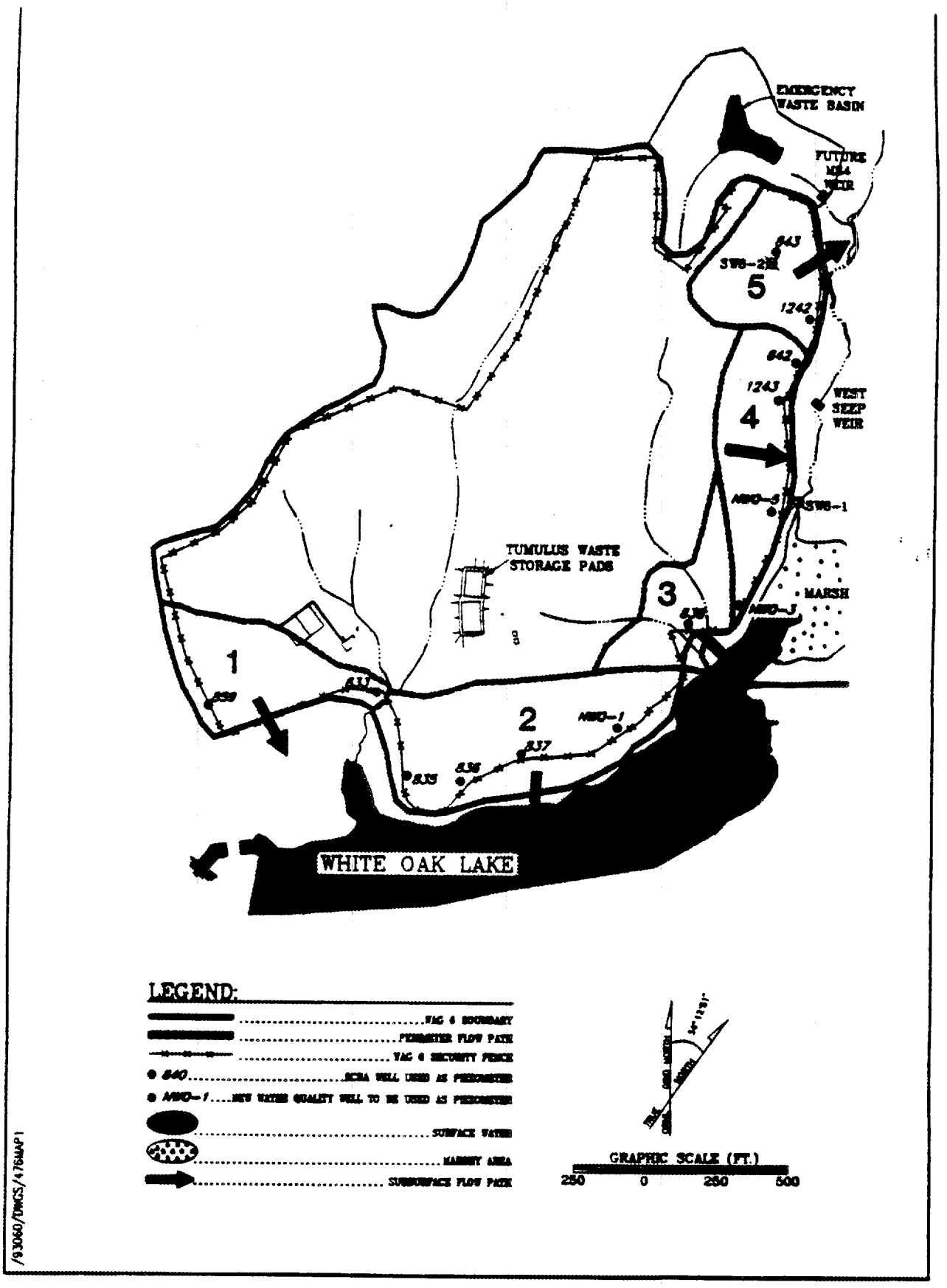

Figure 15. Map of sections used to calculate fluxes along the ungaged perimeter of WAG 6.

The section 4 flux estimate from the WAG 6 model is close to the baseflow (groundwater discharge component) for the West Seep stream gage. Since section 4 is about 1/4 the length of the tributary, it should provide only a portion of the measured baseflow to this tributary, not the entire component. One factor in the high-flux calculations is that the WAG 6 model includes a high-permeability soil zone, but the current version of the MV model neglects this zone. Most of the flux occurs within the top three layers of the WAG 6 model, where the high-permeability zone occurs. This zone is poorly understood, and it is difficult to say whether we can yet assign appropriate parameters (hydraulic conductivity, thickness) to the zone. We should continue to improve models of this zone.

In summary, the fluxes agree quite well in light of the uncertainty of input parameters for the different methods used. Risk assessment modeling, to be conservative, should probably use the highest value calculated, with only small variations ensuing from use of the lower values. However, consideration should be given to use of a lower value for section 4, since the highest value calculated is close to baseflow for the entire reach of the tributary.

Sect #	Clapp	WMV	WMV-XY	ECE
1	0.0011	0.0016	0.0017	0.0012
2	0.0021	0.0042	0.0039	0.0033
3	0.0008	0.0015	0.0012	0.0013
4	0.0011	0.0052	0.0037	0.012
5	0.001	0.00025	0.00015	0.0011

Table 4. Comparison of modeled flux (in cubic feet per second) to the ungaged portion of Waste Area Grouping 6 for alternate models

5. RECOMMENDATIONS FOR FUTURE WORK

Calibration of the Melton Valley groundwater model benefitted from the quick turnaround time provided by P-FEM running on a parallel machine. Further refinement of recharge values, hydraulic conductivities, anisotropy, and boundary conditions will be conducted to improve model calibration. In particular, the detailed data from HHMS-12 and HHMS-13 have not yet been modeled, which when done will test our conceptual model of vertically distributed head data. Sensitivity analysis will be performed to provide error bounds on calculations. Parameters such as anisotropy, recharge, and flux versus no flux boundary conditions will be considered.

In addition, transient simulation of seasonal water level fluctuations; transient simulation of cap response; and smaller scale, unsaturated zone models with highly nonlinear soil moisture curves can be performed with workable runtimes on the supercomputer. Although the current model does not consider stormflow, modeling groundwater fluxes is needed to test hypotheses about the role of stormflow and to help construct boundaries for transient stormflow models.

The model has been expanded to be used as a tool for the entire Melton Valley Groundwater Operable Unit evaluation, so that it now includes WAG 5, WAG 7, and the rest of WAG 2. The new grid has approximately 80,000 nodes and double the area. Some immediate concerns about fluxes in WAG 5 will parallel the work reported here for WAG 6. Modeling of flow in the deep systems will assist efforts to evaluate the short-term versus long-term risks from WAG 10 contaminants, which are believed to be in a slow-moving flow system.

Smaller area models of the stormflow zone have been constructed as a spinoff from this project. Given the fine grids required for unsaturated zone modeling, telescoping models may be the best technique for examining problems in greater detail. Further work is needed to examine what detail can be incorporated in regional models.

6. CONCLUSIONS

Through a better definition of groundwater flow boundaries, the regional model developed here will help identify contaminant pathways and will help researchers understand hydrologic relationships between waste areas in Melton Valley. For example, calculated flow fields can be used to determine whether shallow aqueous contaminants are confined to local flow systems. Although Fig. 10 shows vectors, not pathways, it indicates White Oak Lake discharge to a depth of about 400 ft for the model constructed. True pathway maps can be constructed by integrating and correctly orienting these vector lines. When it should prove necessary to construct a smaller area model, this regional model can suggest appropriate boundary conditions and parameter values, and thus save calibration time. For instance, a fully three-dimensional regional model can be used to evaluate the importance of anisotropy without the influence of local boundary conditions used in a smaller area model.

This model is being used to provide water budgets for calculating contaminant fluxes in the groundwater zone. The model can fill in flux data where gages are not available, thus improving estimates of off-site contaminant migration. These calculations include only saturated groundwater flow, not stormflow and other transient flow.

7. REFERENCES

Borders, D. M, J. A. Watts, R. B. Clapp, B. J. Frederick, S. M. Gregory, T. D. Moore. 1993. Hydrologic data summary for the White Oak Creek Watershed at Oak Ridge National Laboratory, Oak Ridge, Tennessee (January-December 1992). ORNL/ER-166. Oak Ridge National Laboratory.

Dreier, R. O. and L. E. Toran. 1989. Hydrogeology of Melton Valley Determined from Hydraulic Head Measuring Station Data. ORNL/TM-11216. Oak Ridge National Laboratory.

EBASCO. 1993. WAG 6 Interim Remediation Design Criteria Studies: Results of 3D and 2D Groundwater Flow Modeling. Project Order No. 910003.10. EBASCO Services, Oak Ridge, Tenn.

Englund, E. and A. Sparks. 1991, Geo-EAS 1.2.1. EPA-600/8-91/008. U.S. Environmental Protection Agency, Washington, D.C.

Gamliel, A., K. C. Black, and P. M. Craig. 1993. Application of 2D and 3DFEMWATER to assess capping activities for a steeply sloped nuclear waste site, pp. 262-272. In Proceedings of the International Ground-Water Modeling Center Ground-Water Modeling Conference, Golden, Colo. June 1992.

Moore, G. K. 1988. Concepts of Groundwater Occurrence and Flow near Oak Ridge National Laboratory, Tennessee, ORNL/TM-10969. Oak Ridge National Laboratory.

Science Applications International Corporation (SAIC). 1993a. Interim Corrective Measures Cap Evaluation Report for Waste Area Grouping 6 at Oak Ridge National Laboratory, Oak Ridge, Tennessee. ORNL/ER- Oak Ridge National Laboratory.

Science Applications International Corporation (SAIC). 1993b. Environmental Monitoring Plan for Waste Area Grouping 6 at Oak Ridge National Laboratory, Oak Ridge, Tennessee. DOE/OR/01-1192&D1, ORNL/ER-158&D1. Oak Ridge National Laboratory.

Solomon, D. K., G. K. Moore, L. E. Toran, R. B. Dreier and W. M. McMaster. 1992. Status Report, A Hydrologic Framework for the Oak Ridge Reservation. ORNL/TM-12026. Oak Ridge National Laboratory.

Structural Dynamics Research Corporation. 1991. I-Deas Finite Element Modeling User's Guide, Milford, Ohio.

Tucci, P. 1991. Ground-water Flow in Melton Valley, Oak Ridge Reservation, Roane County, Tennessee — Preliminary Model Analysis. USGS Water Resources Investigations Report 85-4221. U.S. Geological Survey, Nashville, Tenn.

Yeh, G. T. 1987. 3DFEMWATER: A Three-Dimensional Finite Element Model of Water Flow through Saturated-Unsaturated Media. ORNL-6386. Oak Ridge National Laboratory.

INTERNAL DISTRIBUTION

L. D. Bates, K-1001, MS-7169
B. A. Berven, 4500S, MS-6124
J. H. Cushman, 1503, MS-6352
V. H. Dale, 1505, MS-6035
E. F. D'Azevedo, 6012, MS-6367
T. O. Early, 3504, MS-6317
D. E. Fowler, 1505, MS-6035
R. L. Graham, 1505, MS-6038
J. P. Gwo, 1503, MS-6352
S. G. Hildebrand, 1505, MS-6037
D. D. Huff, 3504, MS-6317
G. K. Jacobs, 1505, MS-6036
B. R. James, 1503, MS-6352
P. Kanciruk, 1057, MS-6407
G. Mahithakumar, 4500S, MS-6203
D. E. Reichle, 4500N, MS-6253
C. T. Rightimre, 1503, MS-6352
C. H. Romine, 6012, MS-6367
M. E. Sale, 1505, MS-6036
W. E. Sanford, 1503, MS-6352
F. E. Sharples, 1505, MS-6036
S. H. Stow, 1505, MS-6038
L. E. Toran, 1503, ms-6352 (5)
O. R. West, 1505, MS-6036 (5)
M. W. Yambert, 4500N, MS-6243
Central Research Library
ESD Library (15)
Laboratory Records Dept. (2)
Laboratory Record, ORNL-RC
ORNL Patent Section
ORNL Y-12 Technical Library

EXTERNAL DISTRIBUTION

K. C. Black, ECE, Inc., P.O. Box 22668, Knoxville, TN 37922

R. N. Farvolden, Professor, Department of Earth Sciences, University of Waterloo, Waterloo, Ontario N2L 3G1 Canada

D. W. Freckman, Director, College of Natural Resources, 101 Natural Resources Building, Colorado State University, Fort Collins, CO 80523

G. Y. Jordy, Director, Office of Program Analysis, Office of Energy Research, ER-30, G-226, U.S. Department of Energy, Washington, DC 20545

A. Patrinos, Director, Environmental Sciences Division, Office of Health and Environmental Research, ER-74, U.S. Department of Energy, Washington, DC 20585

G. S. Sayler, Professor, 10515 Research Drive, Suite 100, The University of Tennessee, Knoxville, TN 37932-2567

F. J. Wobber, Environmental Sciences Division, Office of Health and Environmental Research, ER-74, U.S. Department of Energy, Washington, DC 20585

Office of Assistant Manager for Energy Research and Development, U.S. Department of Energy Oak Ridge Operations, P.O. Box 2001, Oak Ridge, TN 37831-8600

(2) Office of Scientific and Technical Information, P.O. Box 62, Oak Ridge, TN 37831